Review Article

Liang Gao, Chao Feng*, and Xian Zhao*

Recent developments in terahertz quantum cascade lasers for practical applications

https://doi.org/10.1515/ntrev-2023-0115 received March 28, 2023; accepted August 9, 2023

Abstract: Terahertz (THz) quantum cascade laser (OCL) is an electrically pumped unipolar photonic device in which light emission takes place due to electronic transitions between subbands formed by multiple strongly coupled quantum wells. THz QCL is arguably the most promising solid-state source to realize various THz applications, such as high-resolution spectroscopy, real-time imaging, chemical and biological sensing, and high-speed wireless communication. To date, THz QCLs have covered emitting frequency from 1.2 to 5.4 THz when operating without the assistance of an external magnetic field. The highest output power is in hundreds milliwatt and watt levels continuousmode and pulsed-mode operations, respectively. THz QCLbased local oscillators have been implemented in astronomy for the identification of atoms and ions. However, there are also limitations, including under room-temperature operation, large divergent beam, narrow single-mode frequency tuning range, incomplete polarization control, and narrowrange frequency comb operation that hinder the widespread applications of THz QCLs. Continuous efforts have been made to improve those THz QCL properties in order to satisfy the requirements of different THz applications. This report will review the key output characteristic developments of THz QCLs in the past few years, which aim to speed up THz QCLs toward practical applications.

Keywords: terahertz, quantum cascade laser, far-infrared, intersubband laser

Liang Gao: Center for Optics Research and Engineering, and Key Laboratory of Laser & Infrared System, Ministry of Education, Shandong University, Qingdao, 266237, China, e-mail: gaoliang@email.sdu.edu.cn

1 Introduction

It has long been known that terahertz (THz) region ($\nu \sim 0.3-10$ THz, $\lambda \sim 1,000-30$ µm, and $\hbar\omega \sim 1.2-40$ meV) is ideal in many applications, such as in chemical and biological sensing, imaging and spectroscopic analysis [1–5]. THz radiation can penetrate many non-polar materials, such as plastics, paper, ceramics, wood, and fabrics, that are typically opaque at visible and infrared frequencies. Many molecular species have uniquely strong "fingerprint" signatures at THz frequencies due to the low-energy vibrational and rotational modes that couple strongly to electromagnetic radiation. Fine-structure transitions of atoms and ions are also within THz range. These properties make THz radiation specifically useful in material identification, chemical analysis, and high-resolution spectroscopy in astronomy and plasma science [6–15].

Due to the short wavelength (compared to microwaves) and non-ionized property (compared to high-energy X-rays) of the THz wave, it can be used for non-invasive and high spatial resolution image detection, which matches the requirements of security surveillance, including stand-off imaging for the detection of hidden objects [16,17]. Important applications are also known to exist in biology and medicine [17–19], in areas as diverse as cancer research, DNA sensing, and non-destructive testing of pharmaceutical product. THz source is also expected as carrier to meet the increasing demand for high-speed and high-capacity wireless communications, because the high carrier frequencies promise unprecedented channel capacities [20–23].

In order to unlock the full potential of these applications on a large scale, compact and powerful THz sources are needed. Solid-state electronic devices, such as Gunn oscillators, backward wave oscillators, and Schottky diode frequency multipliers could generate milliwatt (mW)-level average output power for frequencies of approximately 1 THz and below [1,24]. However, the output powers dramatically drop to the order of μ W [25,26] when operating above 1 THz owing to the transit-time and resistance-capacitance effects [27,28]. Optical methods based on photoconductive

^{*} Corresponding author: Chao Feng, Center for Optics Research and Engineering, and Key Laboratory of Laser & Infrared System, Ministry of Education, Shandong University, Qingdao, 266237, China,

e-mail: fengchao@sdu.edu.cn

^{*} Corresponding author: Xian Zhao, Center for Optics Research and Engineering, and Key Laboratory of Laser & Infrared System, Ministry of Education, Shandong University, Qingdao, 266237, China, e-mail: zhaoxian@sdu.edu.cn

effect [29], different-frequency generation (DFG) [30], or optical parametric oscillation [31] can also generate THz radiation; however, those methods require high-energy pump sources, and the whole systems are bulky and power hungry. Recently, a new method relied on DFG in dual-wavelength mid-infrared quantum cascade laser (QCL) has been implemented for THz wave generation, which is currently the unique electrically pumped monolithic semiconductor light source operating at room temperature with widely tunable lasing emission [32-36]. However, the intrinsic low conversion efficiency limits the peak output power only in a few mW for pulsed mode and average power in micro-watt level for continuous-wave (CW) mode [37,38]. Although some THz applications have been realized with the aforementioned electronic and photonic sources, their limitations hinder the further development of THz applications.

The advent of THz QCL in 2002 [39] is a significant breakthrough in the THz field that can potentially bridge the so-called "THz gap" between semiconductor electronic and photonic sources. Till date, THz QCLs have covered frequencies from 1.2 to 5.4 THz (when operated without the assistance of an external magnetic field) [40,41]. The peak output power is 2.4 W at 4.4 THz [42] in pulsed mode at 10 K heat sink temperature and over 100 mW in CW mode [43,44] at 10 K. CW THz QCLs cooled with miniature coolers have been implemented for heterodyne spectroscopy [12–15] and high-resolution absorption spectrometer [9,10] in astronomy and plasma science. The maximum operating temperatures (T_{max}) for pulsed operation of QCLs emitting in the range of 1.5 to 4.5 THz have reached above 150 K with the continuous efforts of systematic optimizing the QCL active region designs [45]. However, the THz QCL operation is still almost restricted to cryogenic cooling; therefore, improving T_{max} to above that of a compact cooler (>235 K for single-stage thermoelectric cooler), or eventually cooler-free, has been a long-term goal in the THz QCL field. Recently, Bosco et al. [46], Khalatpour et al. [47], and Khalatpour et al. [48] reported the small footprint and cryogenic-free THz QCLs with thermoelectric cooler, and the maximum operating temperatures were 201.5, 250, and 261 K, respectively.

Almost all the high operating temperature THz QCLs are based on metal–metal (MM) waveguide owing to the near unit mode confinement factor and good heat removal of bonding metals [46,47,49]; however, the MM cavity is poor emitter due to the large impedance mismatch and subwavelength radiating end-facets. Consequently, QCLs based on MM cavities suffer from low radiative efficiency, highly divergent radiation patterns, and multimode operation [50,51]. In order to improve those properties, different resonator designs, such as distributed feedback (DFB)

grating [52–54], photonic crystal [55], disk [56], two-section resonators [57,58], spoof surface plasmon (SP) structures [59], and beam engineering methods [60], have been developed. Recently, with the development of novel QCL MM cavities, such as vertical-external-cavity surface-emitting laser (VECSEL) [61], phase-locked arrays [62], and photonic wire lasers [63], QCLs with high-power, narrow-beam, and single-mode operation could be obtained simultaneously. Another QCL cavity, SP waveguide, is usually used with external lens to obtain CW operation with high output power and near Gaussian beam profile [11,64].

Frequency tuning and polarization control are also required in many THz applications, such as spectroscopic analysis and circular dichroism spectroscopy. A variety of quasi-static methods to tune single-mode THz QCLs have been discussed in the review article by Vitiello et al. [65]. Thermal tuning [53] and broadly continuous tuning by the use of a mechanical plunger to alter the evanescent optical mode [66] or the external-cavity feedback [67] are investigated. Both of these techniques could only be used for slow tuning speed (few hundred Hz of modulation speed). One time material condensation tuning by modifying the refractive index of the medium surrounding QCL lasers [68,69] and rear-facet illumination by near-infrared (NIR) lasers [70] has also been demonstrated. Fast tuning method, electrical tuning, that induces a change in the effective index of the resonant optical mode is also reported in refs [63,71–75].

THz QCLs naturally emit linearly polarized radiation because of the intersubband transition of electrons in multiquantum wells. Polarization control of THz wave still mostly relies on external modulator elements, such as rotating polarizers/waveplates [76], active THz metamaterials [77,78], and liquid-crystal-based waveplates [79,80]. However, such external controlled approaches will render the system slow, bulky, and expensive. Directly switching the polarization states is always preferred due to the properties such as high speed, compactness, and power efficiency. THz QCL frequency combs have also been developed by engineering the cavity dispersion with different active regions [81-86]. These new comb generators open up novel opportunities for the spectroscopy of molecular fingerprints over broad spectral bandwidths. Realizing THz frequency combs with stable and high output power, as well as entire lasing range comb operation, is preferred for many applications. In this report, we will focus on the key recent developments of THz QCLs in five aspects, namely, CW and high-temperature pulsed operation, highoutput-power and narrow-beam profile, single-mode and frequency tuning, polarization control, and THz QCL frequency combs, which play important roles in practical applications.

2 CW and high-temperature pulsed operation

The CW and pulsed operation of THz QCLs are usually based on different active regions and waveguide designs. There are four different active region designs, namely, chirped superlattice, bound-to-continuum, resonant-phonon, and hybrid design for THz QCLs [2]. The hybrid design can achieve high gain value along with low electrical power dissipation and is usually used for CW operation. The resonantphonon design has clear energy levels and is easier to be optimized for high-temperature pulsed operation. Two different waveguides, SP waveguide [39] and MM [90] waveguide, are developed for THz QCLs. For SP waveguide, the optical mode is vertically confined by a top metal layer and a thin heavily doped bottom contact layer underneath the active region. For MM waveguide, the active region is sandwiched between two metal layers. The optical mode is also confined between these two metal layers. Due to the strong subwavelength confinement, the beam quality and output power of edge-emitting MM QCLs are worse in comparison with those of SP devices. However, MM QCLs have the advantage of operating at higher temperatures.

THz QCLs can provide high output power, narrow linewidth, and high spectral brightness, which are beneficial in high-resolution spectroscopy applications; however, CW operation should be first satisfied [5]. The recorded output power of THz QCLs in CW mode is ~230 mW at 15 K, cooled with continuous-flow liquid-helium [44]. The active region design is based on hybrid bound-to-continuum transition and resonant-phonon extraction scheme, and the device is fabricated with SP waveguide. The operating voltage and current density of the QCL are around 20 V and 600 A/cm², respectively [44]. The ridge dimension is $0.175 \times 2.9 \text{ mm}^2$, so the electrical pump power is calculated to be about 60 W, which is out of the range for mechanical coolers. The reduced thermal conductivity along the growth direction would affect the heat removal of the device, and the wet chemical etching-formed laser ridge would lead to sidewalls and uneven current spreading; these two aspects would make the device not suitable for long time operation and for practical applications.

The need for THz OCLs as local oscillators in heterodyne receivers for astronomy has facilitated the development of low power dissipation CW QCLs. Up to now, THz QCLs have been implemented in high-resolution absorption spectrometers [9,10] as well as in heterodyne spectrometers [5,11-15] for the German Receivers for Astronomy at Terahertz Frequencies (GREAT and upGREAT) on board the Stratospheric Observatory for Infrared Astronomy (SOFIA). The THz QCL local oscillators are compact and can be operated in miniature coolers with typical dimensions of just 100 mm [91]. German Aerospace Center (DLR) demonstrated a CW THz QCL, which was based on the hybrid design and SP waveguide in 2014 [11,64]. The OCL was cooled with the cold finger of a cryocooler (30–80 K), and no liquid cryogens were required. Single-mode emission at 4.745 THz was realized with the first-order lateral distributed gratings, and the output power was 2.2 mW. The emission frequency could be tuned from -1.5 to +6.5 GHz around the center frequency by changing the driving currents. A parabolic mirror was used to obtain near Gaussian beam profile with an M^2 value of 1.2.

The Physikalisches Institut der Universität zu Köln (KOSMA) also demonstrated a single-mode (~6 GHz tuning around center frequency at 4.7448 THz) and MM QCL based on integrated patch antenna arrays [92,93]. The device delivered an output power of 2.4 mW with the fundamental Gaussian mode and was also implemented in SOFIA missions. The other 4.74 THz local oscillator was developed based on an antenna-coupled third-order DFB OCL with MM waveguide for NASA GUSTO project [94,95]. The device was based on the resonant-phonon active medium design. The output power was ~5 mW, and the lasing frequency could be controlled within 1.5-3 GHz around 4.7448 THz. The aforementioned three CW QCLs are all cooled with compact Stirling coolers.

The quantum barrier Al contents of the aforementioned active designs [11,44,64,92-95] are between 15 and 30%, since low-Al contents provide sufficient coupling through thick injection barriers and large tolerance to growth fluctuations. THz QCLs based on binary barrier AlAs have also been demonstrated in the studies by Schrottke et al. [96] and Schrottke et al. [97] in order to realize low power dissipation. By replacing the ternary Al_{0.25}Ga_{0.75}As barriers [98] with binary AlAs barriers and decreasing the barrier thickness correspondingly while maintaining other design parameters approximately similar, the AlAs barrier QCLs showed more than three times higher wall plug efficiency. The threshold current density was also reduced from 350 to 120 A/cm² due to the reduced leakage of carriers through parasitic states. The optimized QCL based on SP waveguide finally operated in CW mode and was used in astronomy applications when cooling with a compact cryocooler.

Besides CW operation, high-temperature pulsed operation is also preferred for many THz applications, such as self-mixing imaging [99,100], spectroscopy imaging [101], real-time imaging [47], and multiheterodyne spectroscopy [102]. Researchers have devoted a lot of effects to increase the maximum operating temperature since the first demonstration of THz QCLs in 2002 [39]. Figure 1 shows the chronological list of maximum operating temperature of THz QCLs. The $T_{\rm max}$ was rapidly increased from 50 to 169 K [39,87,88] in the first 3 years after the demonstration of THz OCL, then slowly improved, and eventually reached to 199.5 K in 2012 [49,51,89]. During this period, active regions with Al_{0.15}Ga_{0.85}As barriers demonstrated better temperature performance than taller barrier designs. Scattering effects were considered to analyze the high-temperature performance, and the conclusion was that tall barriers would introduce large alloy and interface roughness scattering losses compared with shallow barriers, which was detrimental to device performance. However, an insightful discovery found that carrier leakage over quantum barriers was the dominant factor other than scattering effects when operating at high-temperatures [103]. So, by using tall barriers to suppress carrier leakage over the barrier would benefit the T_{max} of QCLs.

Furthermore, the ultimate temperature limit of QCL is also related to the fraction of electron population in the upper state, since parasitic re-absorption of the free electrons and the electrical stability are the key sources of optical losses [104,105]. This leads to the THz QCL design trend to use less number of states per period, which can also be clearly seen from the chronological development of T_{max} in Figure 1. Based on the progress of theoretical works, the highest temperature was finally made a breakthrough to 210.5 K in 2019 [46] and the ultimate temperature was then improved to 261 K in 2022 [48]. The QCL structures in studies by Bosco et al. [46] and Khalatpour et al. [48] both used two-well designs and tall barriers with Al_{0.25}Ga_{0.75}As and Al_{0.35}Ga_{0.65}As, respectively, which were different from the previous maximum temperature designs with relatively low barriers (Al_{0.15}Ga_{0.85}As) and three or more wells per period.

Bosco *et al.* showed the increase of upper laser-state population with the number of active states reduced (Figure 2(a)), calculated with a nonequilibrium Green's

function (NEGF) model for five designs with different numbers of active states per period [46]. The best design (twowell structure) was grown by molecular beam epitaxy (MBE) and processed with MM waveguide. The pulsed L-I-V characteristics from a 1.8 mm × 150 μ m × 12 μ m ridge laser at different temperatures are shown in Figure 2(b). The maximum operating temperature was 209.5 K. The same device was then tested on a four-stage thermoelectric cooler and showed the maximum operating temperature of 210.5 K. Khalatpour et al. increased the maximum operating temperature further to 250 K by using a two-quantum-well design with 30% Al barriers to minimize the leakage channel and realize a clean three-level system, especially at high-temperatures [47]. The conduction band diagram and probability density functions of subband states are shown in Figure 2(c). In order to realize the clean three-level system, reducing intermodule tunneling except for the desired channel $|i_{n-1}\rangle \rightarrow |u_n\rangle$ and reducing the coupling to higher-lying bound states are the two main considerations that need to be satisfied. At operating bias, where $|i_{n-1}\rangle$ and $|u_n\rangle$ are aligned, the higher-energy bound states denoted by $|p_{1,n}\rangle$ and $|p_{2,n}\rangle$ would lie in the continuum and the electron-LO-phonon absorption from $|i_{n-1}\rangle$, $|u_n\rangle$ to $|p_{1n}\rangle$, $|p_{2n}\rangle$ should be minimized. The trade-off between increasing the resonant tunneling between $|i_{n-1}\rangle$ and $|u_n\rangle$ and reducing the leakage to the continuum is the main part of the design effort. Based on these design strategies, multiple QCL active regions were designed and processed, which led to the maximum operating temperature of 250 K. The pulsed L-I performance at different temperatures is shown in Figure 2(d). Real-time imaging with this portable THz system cooled with a thermoelectric cooler and a room-temperature camera was also performed in the study by Khalatpour et al. [47], which was a big step toward THz applications in medicine, biochemistry, and security. The authors further improved T_{max} to 261 K by optimizing the design parameters [48]. Further understanding of the QCL principle such as the role of different scattering

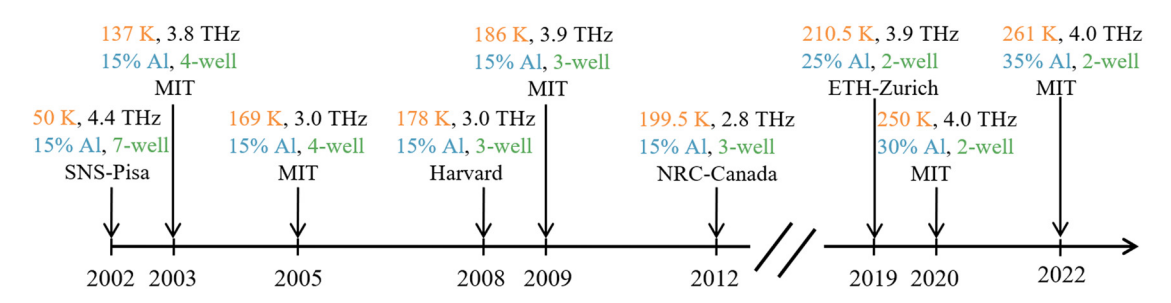


Figure 1: Chronological list of the development of maximum operating temperature of THz QCLs with their lasing frequency, quantum barrier Al composition, number of quantum wells per period, and research groups. These results are summarized from previous studies [39,46–49,51,87–89].

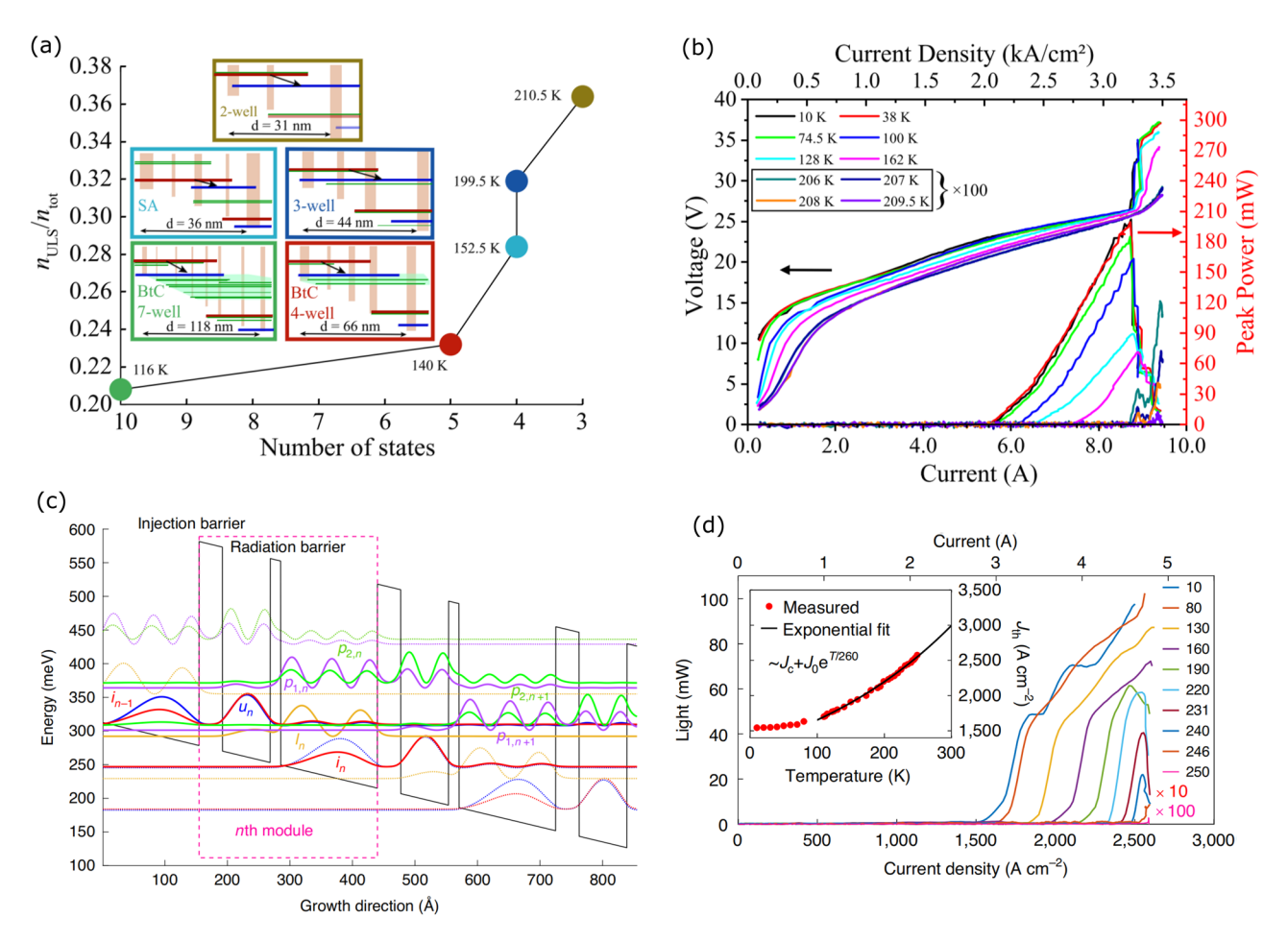


Figure 2: (a) Relative density of the upper laser state of five QCL designs with different numbers of active states per period, simulated with an NEGF model. The upper laser state and the lower laser state are shown in red and blue, respectively. The green lines indicate the other relevant states. The measured maximum operation temperatures are also indicated, respectively; (b) pulsed L–I–V curves at different temperatures of the T_{max} = 210.5 K designs with two quantum wells per period and GaAs/Al_{0.25}Ga_{0.75}As material system. Reprint from ref. [46], (c) probability density functions of subband states of the T_{max} = 250 K designs; and (d) power *versus* current density at different temperatures. Inset: plot of threshold current density *versus* temperatures with T_0 as fitting parameters. The black line is an exponential fit. Reprinted from the study of Khalatpour *et al.* [47].

mechanisms and different leaking channels in the superlattice might bring the THz QCL operating at room temperature in the future.

3 High-output-power and narrowbeam profile

High-power and narrow-beam QCLs are always desirable in many THz applications. For example, QCLs as local oscillators in astronomy applications need to provide large enough power to pump the mixer, as well as to emit with fundamental Gaussian beams to relax the requirements regarding the optics of the spectrometer [5]. THz QCLs with Fabry–Pérot cavity have demonstrated peak output

power in watt level at 10 K by using large and wide laser ridges based on SP waveguide [42,106,107]. Also, the operating temperatures for these devices with an average power of 1 mW are all around 120 K. The beam profile of THz QCLs depends strongly on the type of waveguides, and Gaussian beam can only be realized together with external elements. THz QCLs with SP waveguide have large emission area contributed from the laser ridge and from the substrate, and demonstrate an M^2 value of less than 1.2 when combined with a dedicated lens [11,108,109]. The beam pattern based on MM waveguide is much more divergent due to the highly confined mode between the two metal strips. External elements, such as lens and frequency filter, have to be implemented together in practical applications due to the intrinsic multimode and divergent beam profile of Fabry-Pérot MM QCLs [50,51]. Silicon lenscoupled MM waveguide has shown far-field beam pattern

with a full width at half-maximum value of $\sim 4.8^{\circ}$ [110] and $2.6^{\circ} \times 2.4^{\circ}$ [111], respectively. Several methods have been developed in order to improve the beam profile of QCLs, in particular, QCLs with MM waveguide.

DFB is a routine way to achieve single-mode and tight beam operation for THz QCLs [52-54]. However, the beam divergence of DFB QCLs is usually narrow along the direction parallel to the cavity axis yet highly divergent in the perpendicular direction. Amanti et al. achieved the singlemode operation and narrow-beam profile in two directions (beam divergence of ~10°) simultaneously by using a thirdorder DFB grating to realize k vectors matching of the first and second diffracted modes to the mode in air [54]. This made the diffracted mode propagate in the horizontal direction with a large in-phase cross-sectional area and thus radiate with a narrow far-field beam profile. However, the output powers of DFB THz lasers with normal metal grating periods were still low. In order to improve the output power, Xu et al. implemented a graded photonic heterostructure to excite the radiative symmetric mode in THz QCL and achieved a high peak output power of 103 mW with the beam divergence of 9° × 20° at 20 K [112]. Jin et al. used the second- and forth-order hybrid grating scheme to excite the symmetric cavity mode and

improve the radiative efficiency simultaneously [113]. The device showed a peak output power of 170 mW and single-lobed far-field beam pattern with a divergence of 5 $^\circ$ × 25 $^\circ$ at 62 K.

Coupled cavity is also a promising way to increase the effective emission area of a laser in order to achieve narrow far-field beam pattern. Khalatpour et al. demonstrated a THz laser with a low-divergent beam pattern of 10° and a high output power of 50–90 mW in a CW mode by using coupled photonic wire lasers [63]. This design took advantage of the unique feature of photonic wire lasers, i.e., a large fraction of the mode propagated outside the laser cavity due to the small lateral dimension relative to the wavelength of photonic wire lasers, and used antennacoupled third-order distributed feedback grating (ADFB) as the platform to form the coupled cavity. A periodic antenna-coupled third-order DFB structure, along with the computed symmetric bidirectional radiation pattern, is shown in Figure 3(a). Figure 3(b) shows the L-I-V performance of a representative π -coupled ADFB laser. The radiations from all the antenna loops are in phase along the DFB structure, resulting in a tight far-field beam pattern as shown in Figure 3(c). The same group further improved the beam divergence to 1.4° × 1.8° by using a

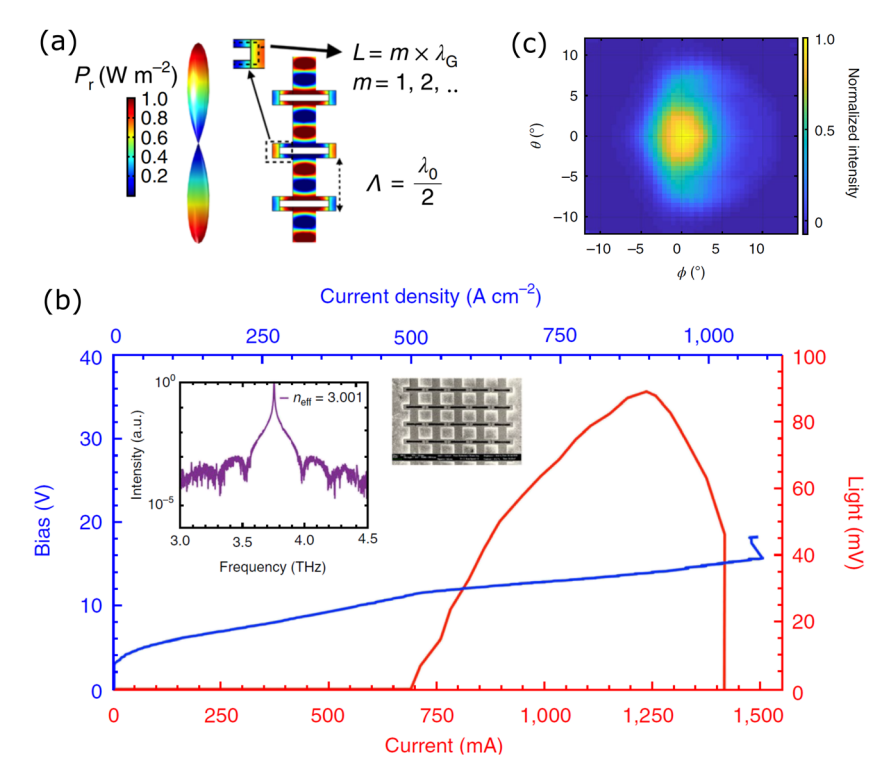


Figure 3: (a) Full-wave simulation of the stimulated fundamental mode and the beam pattern of an ADFB; (b) L–I–V characteristics of a five π -coupled ADFBs when operating in continuous mode. The lasing spectra and SEM image are shown in insets; and (c) and beam pattern of the five π -coupled ADFBs. Reprinted from the study of Khalatpour *et al.* [63].

home-made high-density polyethylene lens mounted in front of the QCL with a distance of 23 mm [114].

Vertical-cavity surface-emitting laser is usually used to achieve narrow beam in visible and NIR range. However, this method cannot easily be applied to QCLs since the intrinsic TM-polarized property (the polarization direction is along the epi-layer growth direction) is due to the selection rule of the intersubband transition. Xu $et\ al.$ demonstrated a metasurface consisting of a subwavelength array of metallic microcavity antennas that could convert the incoming TE-polarized light to the TM-polarized mode (TM₀₁ in this case) in the microcavity. Loading the metasurface with quantum cascade gain material and placing an output coupler created an external laser cavity, which determined the lasing properties, such as output power and beam profile. The novel laser scheme was named as

THz quantum cascade VECSEL, and it showed a near-Gaussian beam of $4.3^{\circ} \times 5.1^{\circ}$ divergence due to the large in-phase emission area [115].

To further increase the output power, Curwen *et al.* demonstrated the THz VECSEL with output power of watt level by using an amplifying metasurface designed for increased power density [61]. Unlike previously demonstrated THz VECSELs [115], the subcavities operated on the third-order lateral modal resonance (TM_{03}), instead of the first-order resonance (TM_{01}), which led to a higher spatial density of the gain material and an increased output power per metasurface area. The transverse field of TM_{03} lateral mode had the same symmetry and coupled to surface incident radiation in the same manner as the TM_{01} ridges, as shown in Figure 4(a). However, since the TM_{03} ridges are approximately three times wider than the TM_{01}

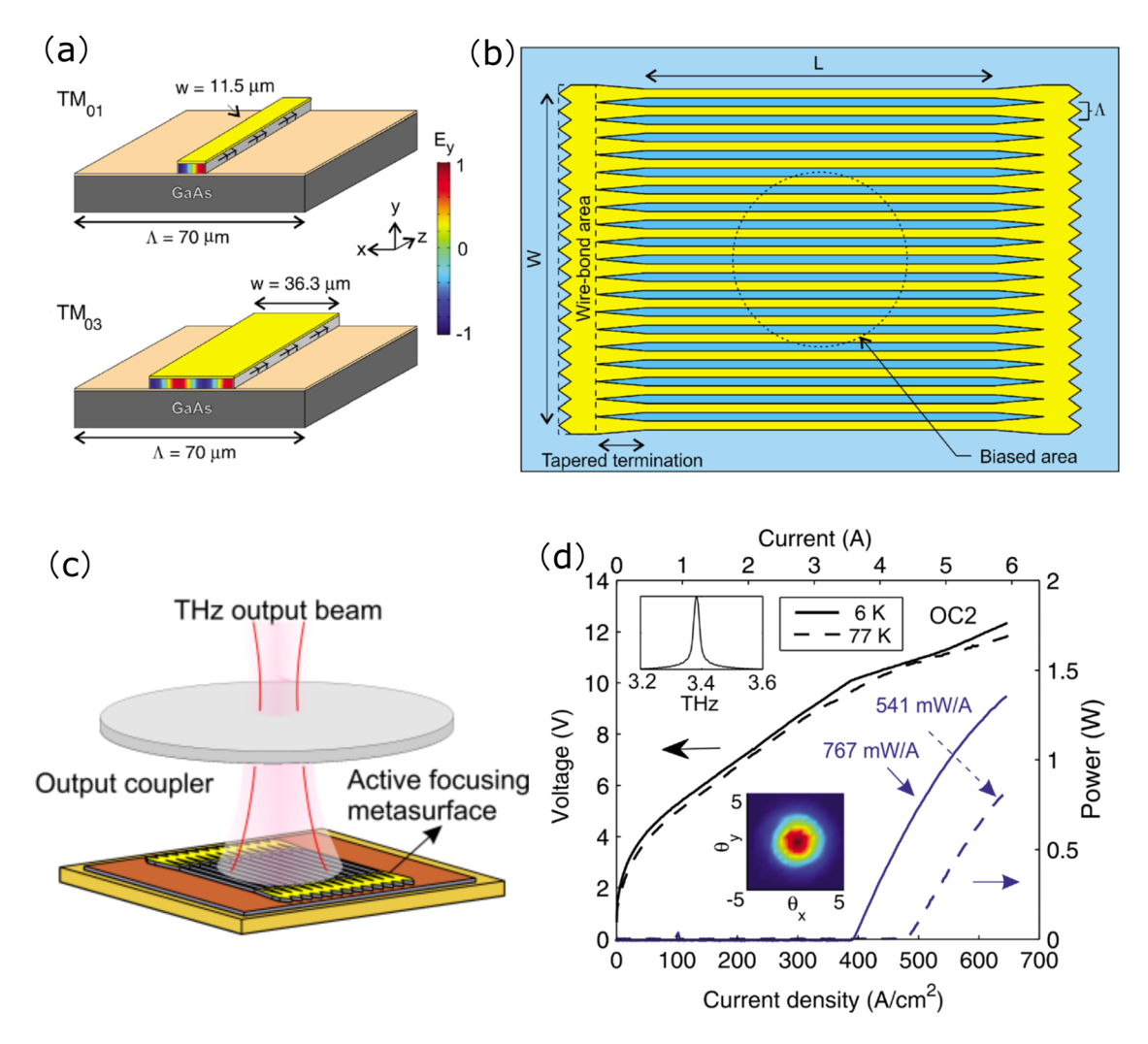


Figure 4: (a) Cross-section of the TM_{03} and TM_{01} metasurface designs; (b) areal view of the TM_{03} metasurface; (c) the THz VECSEL includes an active metasurface and an output coupler; and (d) pulsed L–I–V performance of the TM_{03} VECSEL at 6 and 77 K with the lasing spectrum and beam patterns in the insets. Reprinted from the study of Curwen et~al. [61].

8 — Liang Gao et al. DE GRUYTER

ridges for the same frequency, so the amount of gain material per unit area is increased (Figure 4(b)). The increased "fill factor" would benefit the VECSEL output power without having to increase the overall dimensions of the metasurface and allows for more efficient use of the epitaxially grown wafer. With a low reflectance capacitive mesh output coupler (transmittance of 18%, Figure 4(c)), the device showed an output power of 1.35 W at 6 K and 830 mW at 77 K with a single-mode spectrum and a low divergence beam pattern (Figure 4(d)).

Another method to improve the output power is to increase the power conversion efficiency. The radiative efficiency of Fabry–Pérot waveguide, $a_{\rm rad}$, is typically in the range of 2–3 cm⁻¹ for a 1 mm long MM cavity with emission frequency at 3–4 THz [50], which is much smaller when compared with the total loss coefficient of the laser cavity ($a_{\rm tot}$ is in the range of 10–15 cm⁻¹ [116,117]). Therefore, the radiative efficiency defined as $\eta_{\rm rad} = \frac{a_{\rm rad}}{a_{\rm tot}}$ is much less than 1. Since $a_{\rm rad} \propto \frac{1}{l}$ (L is the length of the laser

cavity), decreasing the cavity length could increase the radiative efficiency. Jin et al. implemented an array of short cavities in a THz plasmonic QCL to improve the radiative efficiency [62]. The microcavities were phase-locked by the established single-sided surface plasmon polaritons (SPPs) in the surrounding medium of the cavities and realized single-mode operation with a peak output power of 2.03 W, a slope efficiency of 1.57 W/A, a peak wall plug efficiency of 2.3%, and a beam divergence of 3.2° × 11.5°, respectively. The concept of phase-locked multiple parallelplate subwavelength metallic cavities, the fabricated device image, and the lasing characteristics are shown in Figure 5. While none of the above-discussed approaches have resulted in an improved beam profile when compared with QCLs with SP resonator together with beam shaping optics, the output powers are significantly improved and the QCLs operate in a robust single mode within the whole lasing range. The beam quality of these QCLs can also be further improved by using external lens as discussed in the study by

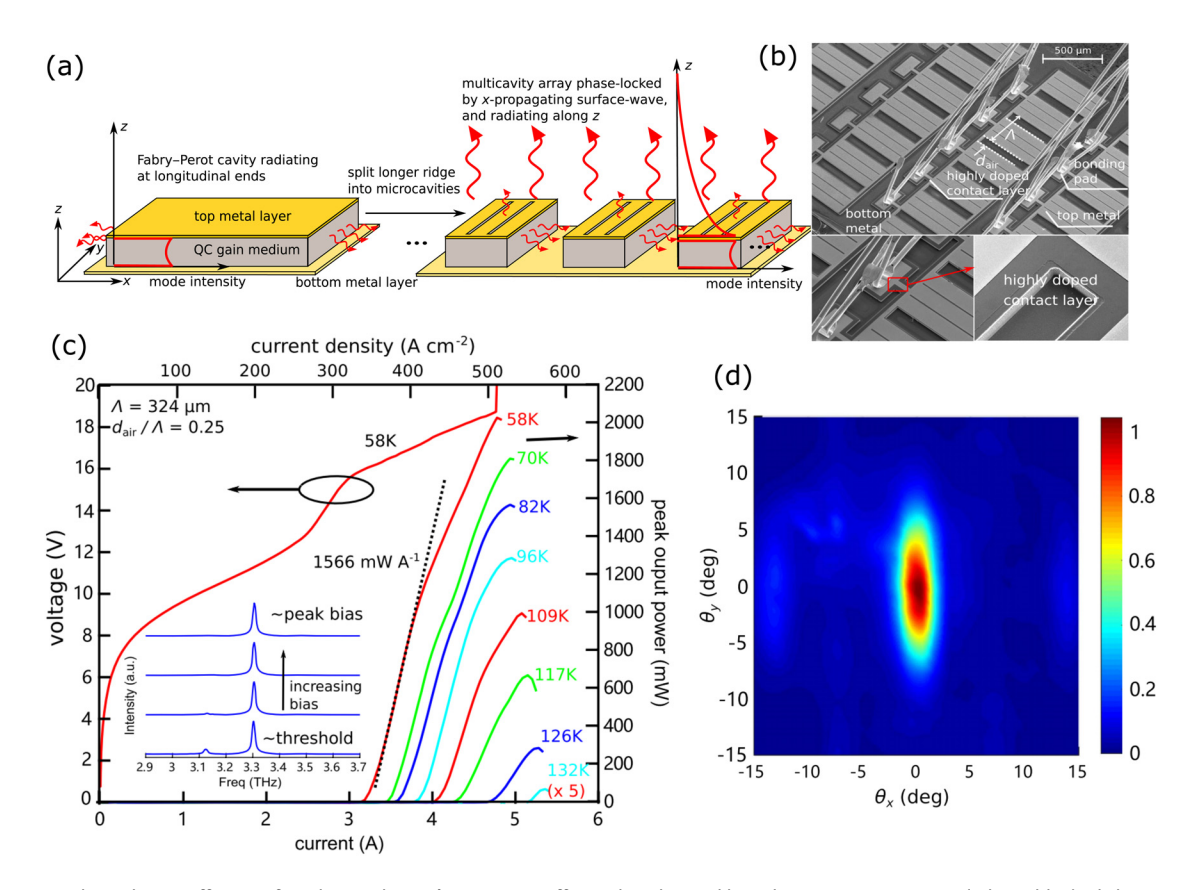


Figure 5: (a) The radiative efficiency for a long Fabry–Pérot cavity is effectively enhanced by splitting it up into several phased-locked shorter cavities. A specific periodic arrangement of the microcavities and slit-like apertures in the top metal layer of the cavities establishes single-sided SPPs in the surrounding medium of the cavities, which leads to phase-locked operation of the microcavities; (b) a SEM image of the fabricated phase-locked QCL arrays; and (c) pulsed L–I–V performance of a representative phased-locked array QCL with seven microcavities at different heat sink temperatures. The inset shows the QCL spectra at different electrical bias at 58 K; and (d) far-field radiation pattern with a divergence of $3.2^{\circ} \times 11.5^{\circ}$. Reprinted from the study of Jin et~al. [62].

Chen et al. [114]. Furthermore, the temperatures for these devices with narrow-beam profile in previous studies [61,62,113] are 77, 99, and 120 K, respectively, when the average output-power is set as 1 mW. The high-power, narrow-beam, and single-mode THz OCLs have important applications in real-time imaging and spectroscopy imaging.

4 Single mode and frequency tuning

THz band is very important in sensing by imaging or spectroscopic analysis since many molecules have strong and distinct spectral signatures at THz frequencies [3]. Those applications need wideband or tunable single-mode THz sources. To achieve the single-mode operation, an effective technique from laser-diode technology, namely, DFB gratings, has been transferred to the THz range. For grating designs of SP waveguide, enhancing the grating contrast for strong feedback at the desired frequency while maintaining the overall loss and confinement factor of the traveling waves within the active region should be considered [91,119,120]. For MM waveguide, large modal effective index contrast can be achieved by creating air slits in the top metal layer without much influence on the overall loss due to the strong mode confinement [52-54,121]. However, non-DFB mode emission and high-order lateral mode oscillation should be prevented by using highly doped GaAs contact layer. Photonic crystals have also been implemented to realize single-mode THz emission [55,122-124]. Robust single-mode operation is also achieved by using two-section resonators [57,58]. The laser is forced to emit at the desired wavelength where the peaks from the two resonator reflection spectra coincide. Recently, the single-mode emission based on GaAs/AlAs heterostructures was also realized with short Fabry-Pérot SP waveguide without any DFB gratings or other wavelength-selection mechanisms [10]. The QCL active regions provide sufficient gain for short resonators so that the mode spacing is larger than the width of the gain spectrum. These short-cavity THz QCLs also demonstrated frequency tuning over 5 GHz with the CW output power higher than 1 mW, which could be used as radiation sources for high-resolution absorption spectroscopy to determine the absolute densities of atoms and ions in plasmas. However, the exact lasing frequency of a FP resonator depends sensitively on the exact length of the resonator, which imposes a challenge for cleaving a laser bar. Another method to obtain exact frequency is to precisely adjust the cavity length after cleavage by polishing the ridge facets [125]. The short-cavity structure is advantageous in its simpler fabrication as it does not need additional wavelength-selection structures, but the short FP cavity length also limits the output power and frequency tuning range of these lasers.

QCLs are particularly suitable for broadband tuning because the gain material can be engineered to exhibit up to octave spanning bandwidths [81]. The tuning ranges based on temperature change are relatively narrow, typically in the order of a few GHz, and the typical tuning rates are several tens of MHz/K or a few MHz/mA [65]. Also, the thermal tuning speed is inherently slow. Tuning scheme through electromechanical movement is beneficial in broadband and continuous tuning; however, it suffers from problems such as bulky size, mechanical instability, and slow tuning speed. Qin et al. demonstrated a singlemode QCL with broad continuous tuning range covering the entire laser gain spectrum (130 GHz tuning with mode hopping) [66]. This method used a narrow strip ($w \approx \lambda/3$, where w is the cavity transverse dimension) MM geometry with first-order DFB grating to force single-mode operation while modifying the lasing mode index by changing the transverse vector through mechanically bringing the plunger close to the side of the laser ridge. The device setup is shown in Figure 6(a). The same group later obtained a continuous and reversible tuning range of 330 GHz [118] by using a narrower wire laser with $w = \lambda/8$, and the tuning result is shown in Figure 6(b).

The THz VECSEL is also desired to realize frequency tuning by changing the length of the laser cavity since it allows for subwavelength-sized cavities. In order to realize broadband continuous tuning and avoid mode hopping, the laser cavity is kept optically short to ensure a large free spectral range compared to the gain bandwidth of the amplifying material. Curwen et al. presented a THz VECSEL, which exhibited ~650 GHz frequency tuning of a single lasing mode (Figure 6(c)) by mounting an active reflect array metasurface and a piezoelectric stepper motor to control the position of the output coupler entirely in the vacuum cryostat [67]. Furthermore, the radiating aperture of VECSEL is in millimeter scale, which is much larger than the normal QCL emitting facet with micrometer scale; this allows the generation of near diffraction limited beams and high output power. Therefore, good beam quality and high output power are obtained simultaneously in THz VECSEL, as shown in Figure 6(d).

The tuning speed of the aforementioned methods is relatively slow, which limits the applications requiring fast scanning speed. The most common mechanism to tune a THz QCL fast is by using the inherent blue shift in the peak frequency of the intersubband gain of a QCL with

10 — Liang Gao et al. DE GRUYTER

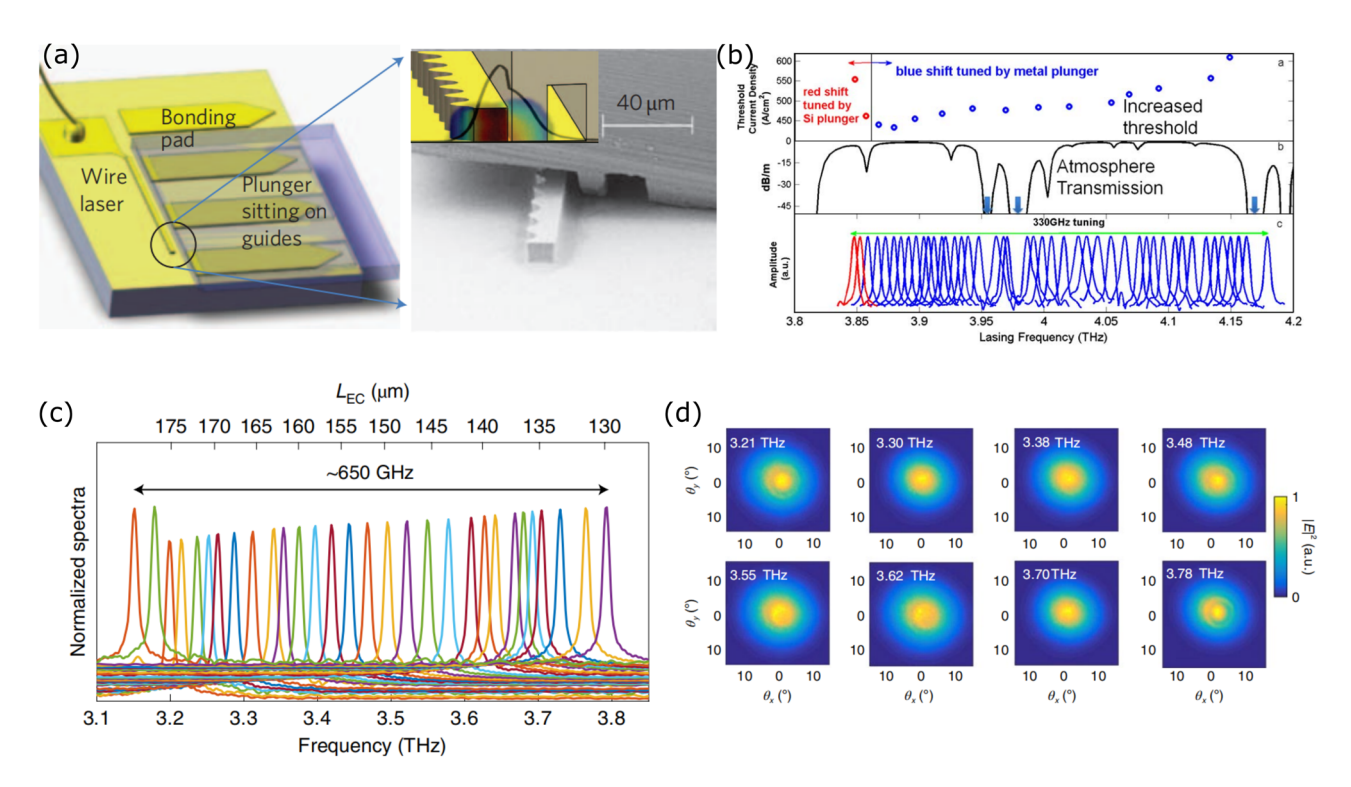


Figure 6: (a) Experimental setup of a THz wire laser with a frequency-tuning plunger. The enlarged figure is a MM ridge waveguide with sinusoidal corrugations on one side to provide first-order DFB to realize single-mode operation; (b) 330 GHz continuous frequency tuning from a THz wire laser (bottom row), the gaps in the tuning spectra are attributed to the strong atmosphere absorption as indicated in the atmospheric transmission spectrum (HITRAN 2008) in the middle row. The top row is the threshold current densities at different frequencies; (c) frequency tuning range of the THz VECSEL by varying the cavity length; and (d) beam patterns measured at different lasing frequencies; (a) Is reprinted from the study of Qin et al. [66], (b) from the study of Qi et al. [118] and (c) and (d) from the study of Curwen et al. [67].

higher voltages due to the Stark effect in the quantum wells. Tuning by Stark effect is an ultrafast electro-optic method that is limited in speed only by the electrical time constant of the modulation response of a QCL cavity [128]. By changing the driving currents, the CW QCLs discussed in Section 2 demonstrated 3–8 GHz frequency tuning range [10,64], where the output power varies for different frequencies. The π -coupled ADFB QCL (Figure 3) also realized 10 GHz frequency tuning with the bias current changing. However, instabilities such as mode jumping and discontinuous changes of output power have to be avoided for the entire tuning range.

Fast and continuous tuning of THz QCLs based on single-plasmon waveguide has also been demonstrated by illuminating the rear facet of the FP cavity with an NIR diode laser (DL) [58,70,126]. The frequency tuning was attributed to the optical excitation of an electron–hole plasma, which changed the refractive index of the QCL medium. As shown in Figure 7(a), one facet of the QCL is illuminated with an NIR diode laser. The emission of the DL is focused with a 30 mm lens and a tenfold objective into a 90 μm spot and then is aligned on the substrate of the

QCL facet, as shown in Figure 7(b). For SP waveguide, a large partial of the mode intensity is located within the GaAs substrate. Hence, manipulating the optical properties of the substrate will change the behavior of the QCL. Single-mode frequency tuning of almost 40 GHz was achieved for a QCL emitting at around 3.1 THz when operating in CW mode. The entire tuning system is compact and low power consumption and has been established to measure methanol transmission spectrum, as shown in Figure 7(c). Depending on the sweep rate, the acquisition of a single spectrum takes typically 20–100 ms.

Electrical frequency tuning of pulsed THz QCLs has also been studied. Turčinková *et al.* [74] reported an electrically tunable THz QCL by using a two-section (master and slave section) longitudinal interdigitated third-order DFB cavity (Figure 8(a)). 4 GHz frequency tuning with constant power of ~0.7 mW at 10 K as shown in Figure 8(b) was realized by changing the currents of the master and slave section of the DFB laser. Kundu *et al.* implemented coupled Y-branched THz QCLs to realize electrical frequency tuning based on the Stark shift and the cavity-pulling effect [75]. Each cavity of the Y-branched QCLs

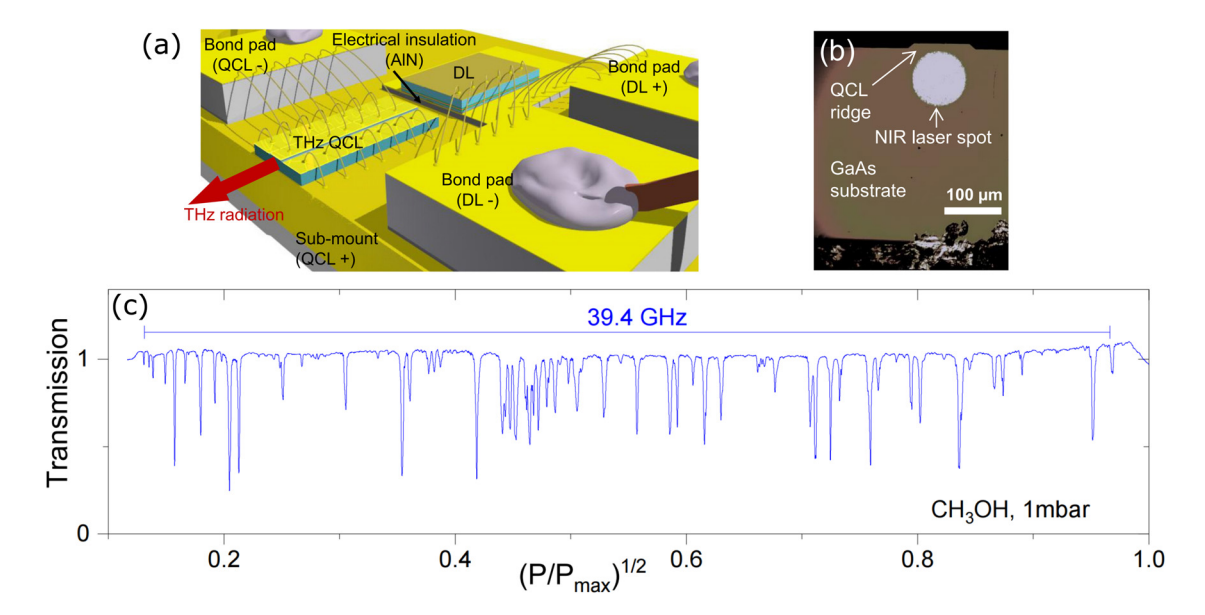


Figure 7: (a) Schematic of the compound structure with the QCL and the DL, the confocal microscope setup is not shown in this figure; (b) microscope image of the illuminated QCL facet; and (c) measured methanol transmission spectrum with a near 40 GHz tunable QCL. The transmission is displayed *versus* the square root of the normalized DL power. Reprinted from previous studies [70, 126].

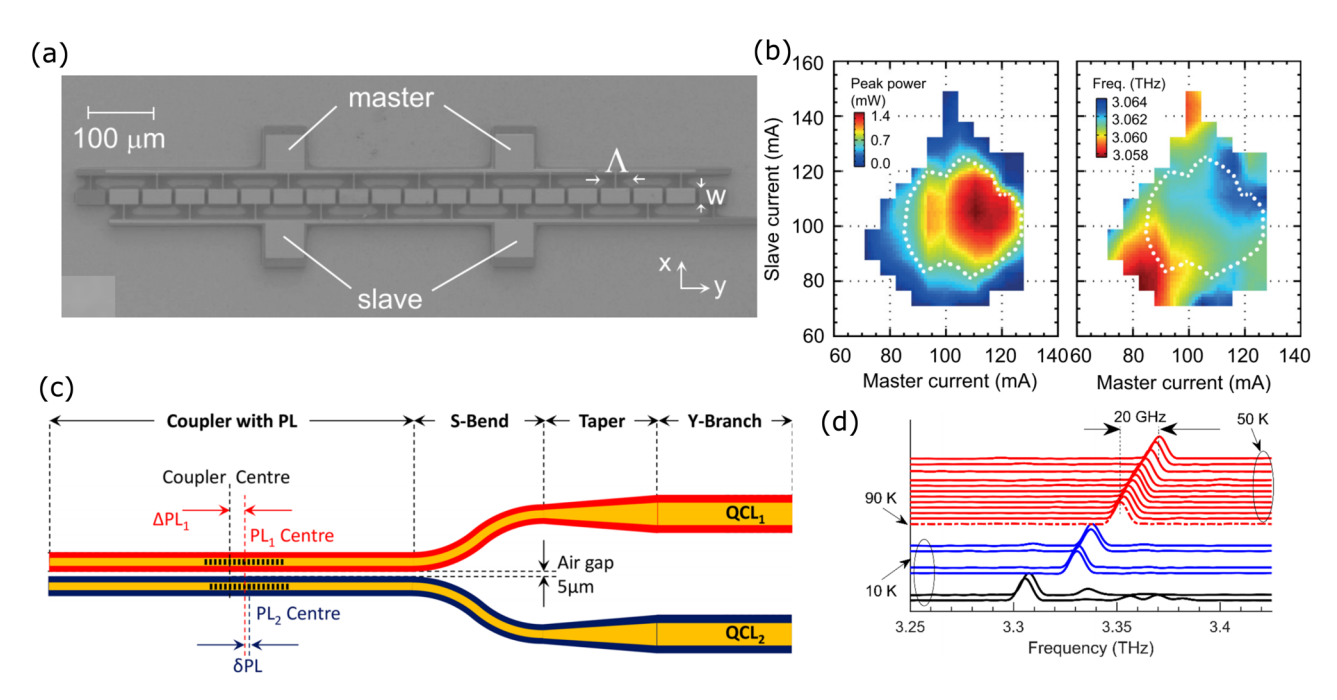


Figure 8: (a) SEM image of the two-section interdigitated DFB THz laser. The two sections are named as master and slave, respectively; (b) output power and frequency of the laser mode as a function of the master and slave currents; (c) schematic illustration of two optically coupled THz QCLs with integrated photonic lattices to engineer the spectra in individual cavities; and (d) representative spectral coverage obtained by varying the current of both QCLs at different operating temperatures. (a) and (b) are reprinted from [74] and (c) and (d) from ref. [75].

includes four different functional sections and a photonic lattice to control the lasing spectra as shown in Figure 8(c). By changing the applied biases of the two QCLs, the device showed 19 GHz frequency tuning range with near constant power of ~4.5 mW at 50 K (Figure 8(d)). The same group

lately demonstrated frequency tuning over 209 GHz including mode hop-free continuous tuning of \sim 6–21 GHz across six frequency bands, controlled through the Stark shift, cavity-pulling, localized Joule heating, and thermal effects [129].

Recently, an electro-optically tunable THz QCL operating close to its peak bias was realized by changing the refractive index of the QCL active region based on "detuned intersubband absorption" [127]. The absorption transition occurs below threshold as opposed to the aforementioned threshold tuning due to the Stark shift in the gain spectrum. A frequency-detuned intersubband absorption transition is specifically implemented via bandstructure design as shown in Figure 9(a) and (b). The frequency of the peak of absorption transition is appropriately detuned from that of peak gain transition (by ~0.3 THz here) such that it has a negligible detrimental impact on the gain at the lasing frequency but still has a substantial effect on refractive index of the superlattice medium at that frequency, which leads to frequency tuning by the cavity-pulling effect. Two optically coupled but electrically isolated cavities (Figure 9(c)) were used to realize approximately 4 GHz electrical tuning (Figure 9(d)) for a 3.6 THz DFB QCL with near-constant peak power in the range of 5-5.3 mW and in a narrow

single-lobed beam with far-field divergence of $\sim 4^{\circ} \times 11^{\circ}$ (Figure 9(e)).

5 Polarization control

Polarization is an important aspect of any light source, and the ability to control the polarization states of the laser output beam is essential for many applications, such as polarization-sensitive imaging, vibrational circular dichroism spectroscopy, and ellipsometry. For THz QCLs, the output polarization can be altered through the interaction of the electric field with the emission apertures, by implementing DFB metal gratings or antennas to achieve linear polarization. However, circularly or elliptically polarized states cannot be realized with those methods. Rauter *et al.* obtained circularly polarized laser by patterning surface-emitting gratings comprising sets of orthogonally

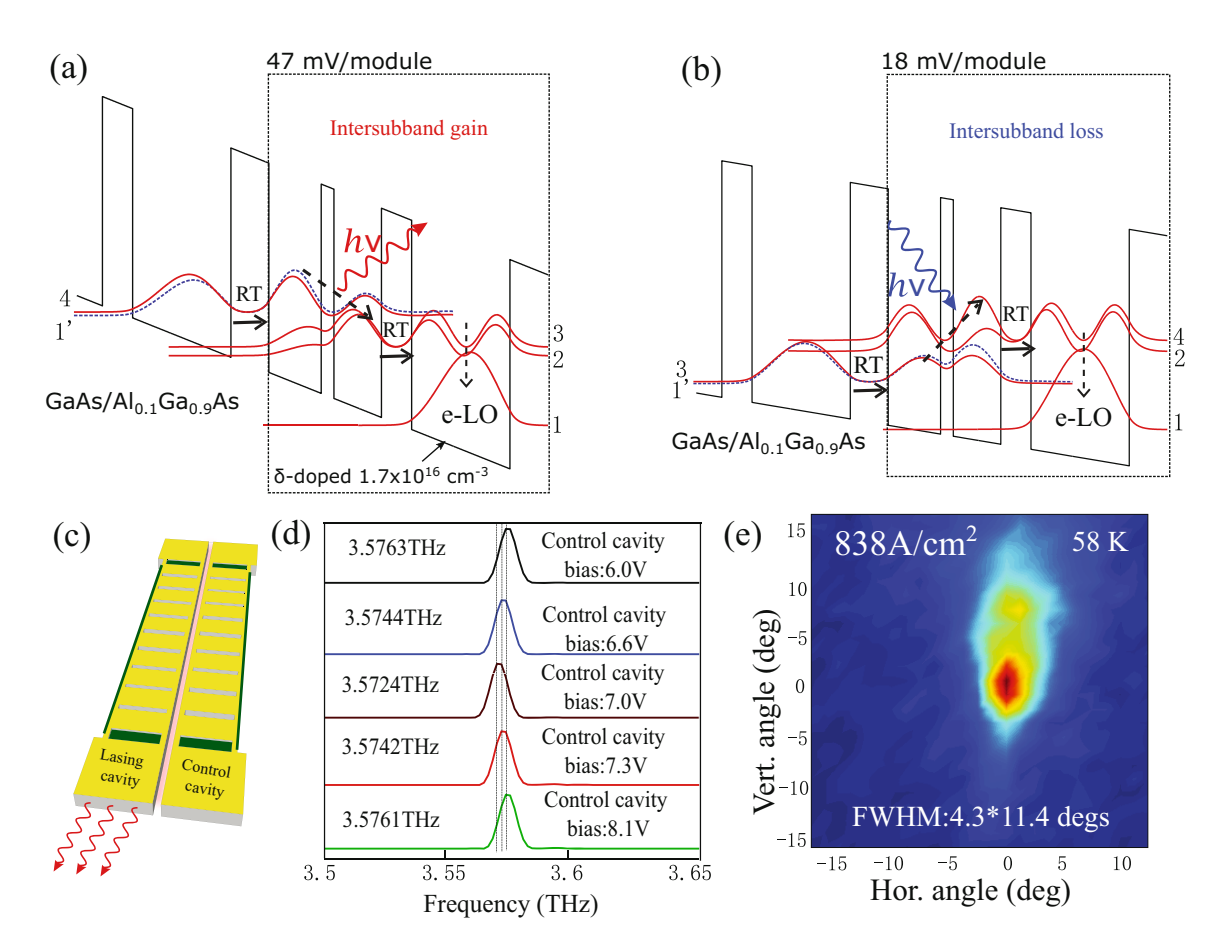


Figure 9: (a) Conduction band diagram at bias corresponding to peak gain for the tunable THz QCL; (b) conduction band diagram at lower bias corresponding to loss transition for the same QCL structure; (c) bias setup of two laterally coupled DFB cavities, (d) the emission spectra of the lasing cavity operated at peak bias, while the bias of the control cavity is varied; and (e) far-field radiation pattern of the lasing cavity with the divergence of $4^{\circ} \times 11^{\circ}$. Reprinted from the study of Vitiello and De Natale [127].

oriented aperture antennas [134]. With different grating designs, a series of polarization states, from linear to elliptical, were observed. Degrees of circular polarization as high as 98% were demonstrated yet only for selected far-field regions and within a collection half-angle of about 6°. Zhu et al. reported the polarization-controllable THz source based on single-mode master oscillator power amplifier (MOPA) [130]. The MOPA device was composed of a first-order DFB laser as the master oscillator, a preamplifier, and a 2D periodical antenna array as the power extractor. The polarization state was determined by the orientation and phase relationship between the 2D antennas. The degree of linear or circular polarization reached as high as 97.5 or 99.3%, respectively, by choosing different antenna orientations and periods. Figure 10(a) shows the scheme of the MOPA device based on MM waveguide. The SEM image shows two antenna arrays with orthogonal orientations. Figure 10(b) and (c) demonstrates the beam profiles of two representative devices (both with divergence of 25° × 33°) with different polarization states and the collected power

through the polarizer *versus* its orientation angle on different spots of the beam patterns.

Borrowed the fundamental mechanism used for beam shaping in radio frequency phased-arrays, ref. [131] demonstrated a THz laser that could be designed to radiate with any coherent polarization states from linear to circular. The laser included arrays of 10×10 patch antenna microcavities and radiated with single-mode frequency, up to 25 mW output power, and narrow beam with divergence of $2^{\circ} \times 2^{\circ}$ simultaneously. By interconnecting the symmetric square microcavities with narrow plasmonic wires along one direction as shown in Figure 10(d), the resonant frequency detuning between the TM modes (TM_{10} and TM_{01}) was introduced. This feature allowed devices to be designed to radiate with any coherent polarization states from linear to circular. Combining different design parameters s and d enabled different polarization scheme as observed in Figure 10(e).

However, the polarization properties based on the aforementioned methods are fixed after fabrication. Liang *et al.* implemented two side-by-side phase-locked tapered

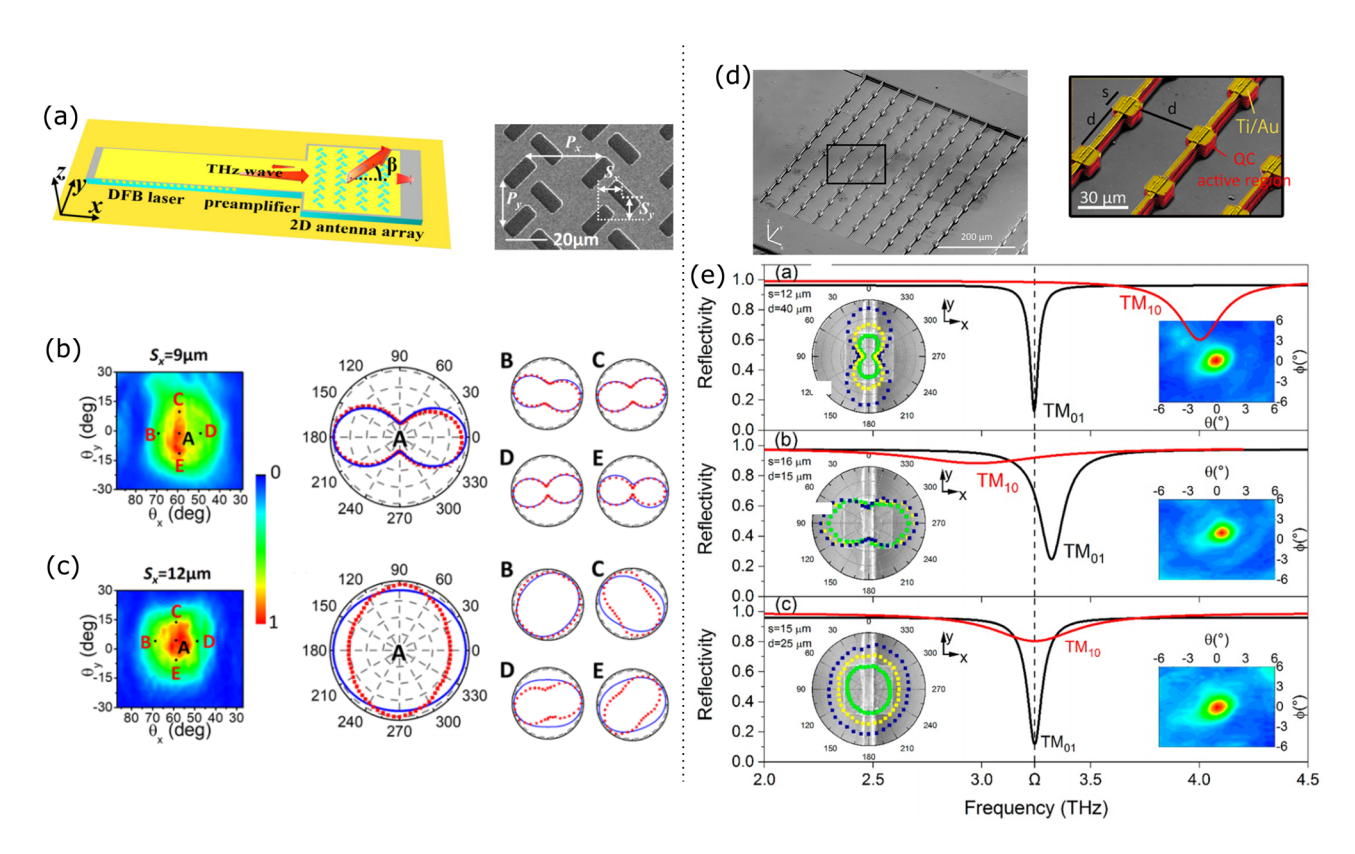


Figure 10: (a) Schematic illustration and SEM image of the THz MOPA QCL with controllable polarization; (b) and (c) measured far-filed beam patterns and the collected power *versus* the orientation angle of the polarizer at different spots on the beam patterns of two representative devices. The measured results are in red dots, while the simulated results in blue curves; (d) SEM image and design parameters, *s* and *d*, of the fabricated 10 × 10 patch-antenna arrays; and (e) simulated reflectivity spectra, measured polarization state, and measured far-field beam patterns of three representative samples with different array parameters *s* and *d*. (a), (b), and (c) are reprinted from the study of Zhu *et al.* [130] and (d) and (e) from the study of Pérez-Urquizo *et al.* [131].

QCLs with dielectric-loaded SP waveguide to first realize dynamically polarization control [132]. By injecting two coherent beams into two orthogonal antenna arrays arranged in a second-order grating and manipulating the intensity of each beam, QCLs showed dynamically tunable polarization from linear to circular. The system architecture is shown in Figure 11(a). A continuous tuning of output beam polarization from linear to near-circular state with the pump intensity of one laser is fixed, while another one varied, as shown in Figure 11(b). Xu et al. demonstrated a THz VECSEL with electrically controlled switching between two linear polarizations separated by 80° [133]. This was enabled by integrating a polarization-sensitive metasurface with a semiconductor gain medium to selectively amplify a cavity mode with the designed polarization state, therefore leading to an output in desired polarization. The polarization-sensitive metasurface was composed of two interleaved arrays of surface-emitting antennas, all of which were loaded with quantum cascade gain materials (Figure 11(c)). Each array was designed to resonantly interact with one specific polarization; when electrical bias was selectively applied to the gain material in one array, selective

amplification of one polarization occurred. Figure 11(d) demonstrates the 80° linear polarization angle switching when biasing the two arrays separately. The VECSEL also simultaneously showed excellent beam with a narrow divergence of $3^{\circ} \times 3^{\circ}$ and a peak output power of 93 mW at a temperature of 77 K.

6 THz QCL frequency combs

THz frequency comb has many applications in dual-comb spectroscopy, quantum metrology, hyperspectral imaging, molecular sensing, and quantum science and technology. THz QCL frequency combs with stable and high output power and entire lasing range comb operation are preferred for applications. Frequency combs based on THz QCLs have been demonstrated with heterogeneous [81–83,135] or homogeneous [84–86] active region designs. THz QCL comb formation is due to the large third-order $\chi^{(3)}$ Kerr nonlinearity of the QCL gain medium, which, in turn, determines a robust interaction between adjacent modes via the four-wave

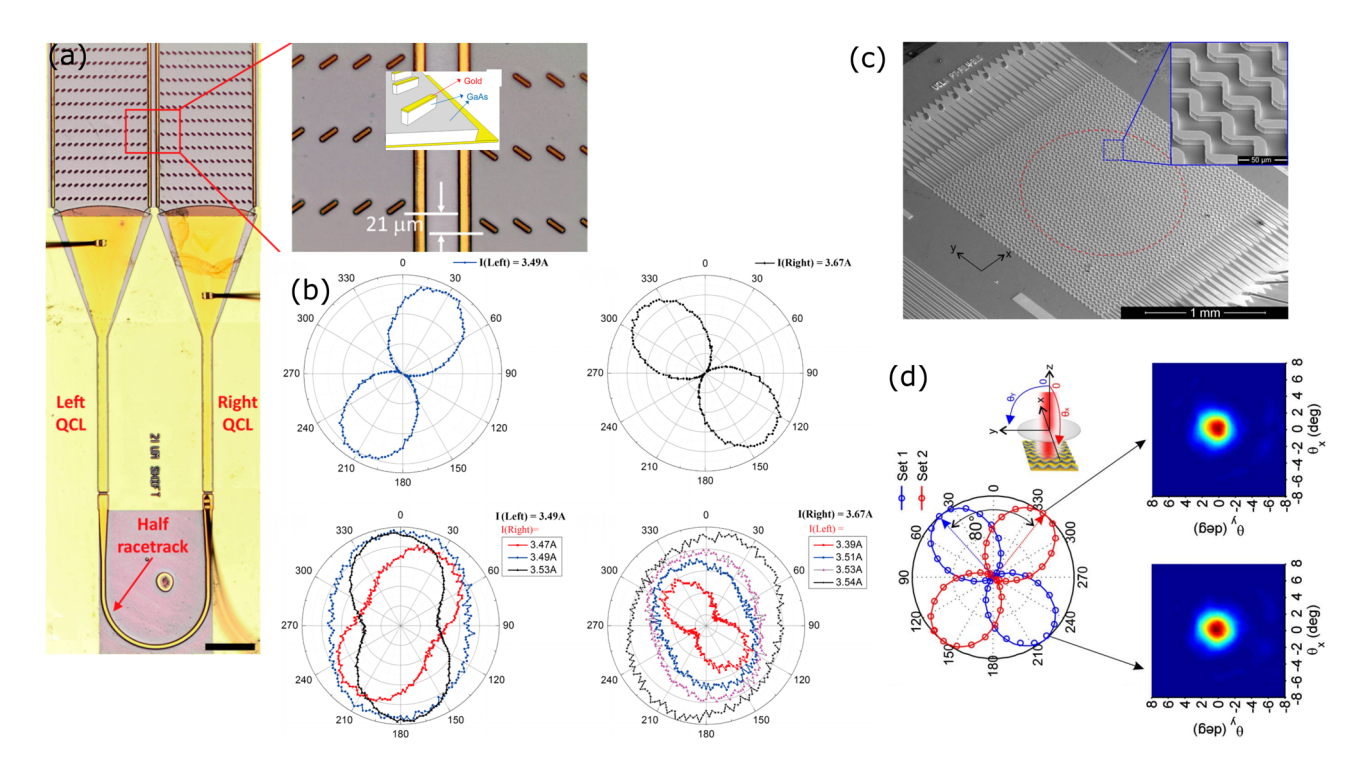


Figure 11: (a) Optical microscope image of the polarization controllable THz QCLs. The two sets of cross-oriented antenna arrays are vertically offset by 21 μm, corresponding to a phase shift of $\sim \pi/2$. The enlarged inset shows the schematic of the antennas; (b) polarization states of the phase-locked QCLs when only the left or right arm is biased at certain current, and the evolution of the polarization state when varying the injection current of one arm while keeping that of another arm fixed; (c) SEM image of the polarization controllable THz VECSEL. The inset shows the zoomed zigzag metasurface; and (d) total output power through the polarizer *versus* the polarizer angle for the two sets of interleaved arrays of antennas. 80° linear polarization angle switching is shown by the arrow. The far-field beam patterns of these two sets are shown correspondingly. (a) and (b) are reprinted from the study of Liang *et al.* [132] and (c) and (d) from the study of Xu *et al.* [133].

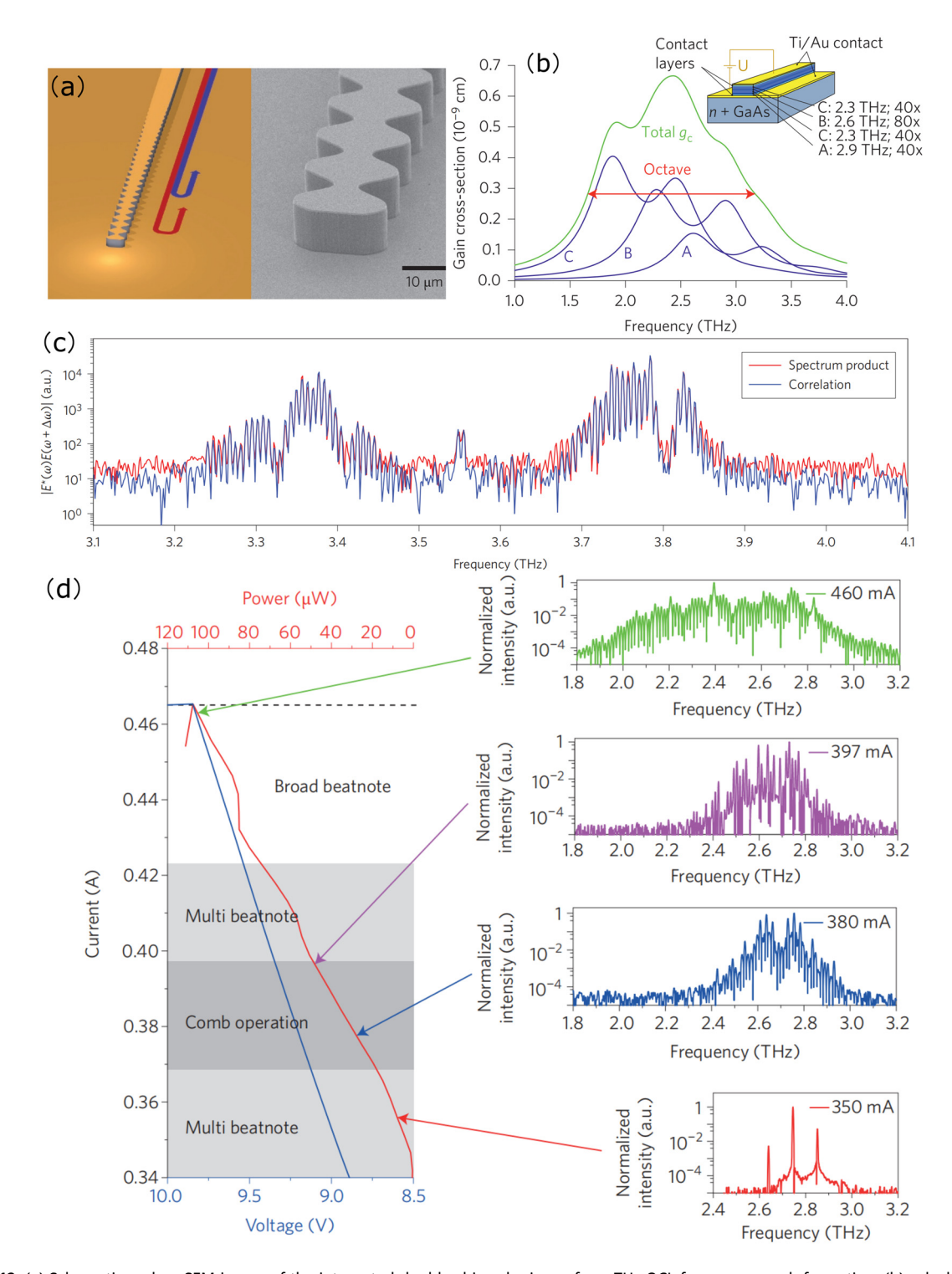


Figure 12: (a) Schematic and an SEM image of the integrated double-chirped mirrors for a THz QCL frequency comb formation; (b) calculated gain cross-section of a heterogeneous THz QCL; blue curve for individual active region design labeled as A, B, and C; green curve for total active region; (c) optical spectrum and correlation spectrum of the THz QCL frequency comb; (d) left panel: beatnote analysis along the LIV range of a THz frequency comb with the shaded area indicating the comb region, in the light gray area, subcombs are observed; right panel: spectra for different currents. (a) and (c) are reprinted from [84] and (b) and (d) from [81].

mixing (FWM) process [136–138]. However, in a free-running THz QCL, the modes are not uniformly spaced, due to chromatic dispersion [84,139]. The interplay between FWM and

group velocity dispersion (GVD) in the laser cavity plays a major role in determining the frequency comb stability over the lasing range. Gain medium engineering can indeed allow a flat top gain [81], but only at a specific bias point. Stable comb operation is only observed over a partial operational current range in which bias-depended chromatic dispersion is compensated, since most dispersion compensation mechanisms in the THz range are not tunable [81–84].

Burghoff et al. [84] demonstrated the first THz QCL comb by integrating dispersion compensation into the OCL waveguide to cancel cavity dispersion. The schematic of the frequency comb is shown in Figure 12(a). Seventy spectral lines spanning a total range of 500 GHz was realized as shown in Figure 12(c); the frequency comb operation range was ~29% of the laser operation range. The optical power was not nearly constant as the MIR QCL combs because THz frequency combs have complex temporal structures [139]. By using a heterogeneous active medium where three different active region designs were stacked together as shown in Figure 12(b), an ultrabroad frequency comb spreading a spectral range as wide as 624 GHz in an octave-spanning THz QCL was demonstrated [81]. The broad gain curve is favorable for comb operation since it results in a low gain GVD. The frequency comb operation range was ~36% of the laser operation range as illustrated in Figure 12(d). Yang et al. [140] obtained frequency comb operation over the whole bias range by using an external cavity to dynamically compensate bias-dependent dispersion. However, the optical bandwidth was reduced and output power was limited to µW level. Up to now, dual-comb spectroscopy based on THz QCLs has been investigated to detect gas with high temporal resolution [102,141,142]. Yang et al. [102] demonstrated the first multiheterodyne spectroscopy using two THz QCL combs. The average signal-to-noise ratios of 24 dB over a spectral range of 250 GHz in just 100 µs was achieved. Broadband transmission spectrum of etalon samples was measured with the THz QCL comb. Consolino et al. showed a metrological-grade hybrid dual-comb spectrometer based on multi-heterodyne down-conversion of a THz QCL frequency comb and a fully stabilized optically rectified THz frequency comb. Methanol molecular transition was measured and matched well with currently available molecular database [141]. Multiple molecular detection in gas phase was reported in the study by Sterczewski et al. [142] based on dual-comb spectroscopy with continuously evolving spectra from gas mixtures with 1 ms temporal resolution. Accurate and fast control of the comb line positions will benefit dual-comb spectroscopy in the THz range, which is still largely unexplored and is open to new insights and improvements.

Achieving THz QCL frequency comb operation over the entire lasing range with high output power and broad spectral coverage is very challenging. Recently, THz QCL frequency combs based on other emerging approaches such as harmonic comb regime [143], grating-gated modulator used with graphene as passive dispersion compensator [144], graphene saturable absorber reflector [145], and integrated intersubband polariton bleaching [146] have been demonstrated and discussed in detail in the study by Vitiello *et al.* [147].

7 Conclusion

Since the first demonstration in 2002, THz QCLs have experienced rapid development and become the most promising candidate to realize the important and unique applications in the THz field. THz QCLs operated in CW mode with several GHz tuning range and Gaussian beam profile have been implemented as local oscillators for highresolution heterodyne spectroscopy. The remarkable progress in maximum operating temperature made THz QCLs operate cryogenic-free which would open up new applications requiring portable high-power THz sources. Dualcomb spectroscopy based on THz QCLs has been used to detect multiple molecular samples. However, much efforts still need to be devoted to comprehensively understand the underlying physics of THz QCLs to further improve their properties. The developments of new materials, such as GaN/AlGaN [148-150] and Ge/SiGe [151,152], might impact THz QCL domain further and become the potential candidates for the next generation of THz QCL active regions. Combining with 2D materials [153] will improve the modulation properties of THz QCLs, which are desired in THz communications. Monolithic THz QCLs that simultaneously include high output power, good beam quality, wavelength and polarization controllable, and cryogenic-free operation might be realized in the near future and enrich the physics and widespread applications of THz QCLs.

Funding information: This work was funded by the China Postdoctoral Science Foundation (No. 2022M711896) and the Natural Science Foundation of Shandong Province (No. ZR2022QF007, ZR2023MF050).

Author contributions: All authors have accepted responsibility for the entire content of this manuscript and approved its submission.

Conflict of interest: The authors declare that they have no conflict of interest.

References

- Tonouchi M. Cutting-edge terahertz technology. Nature Photonics. 2007;1:97-105.
- [2] Williams BS. Terahertz quantum-cascade lasers. Nature Photonics. 2007;1(9):517.
- Mittleman D. Sensing with terahertz radiation. Berlin, Heidelberg: [3] Springer; 2013.
- [4] Siegel PH. THz instruments for space. IEEE Trans Antennas Propag. 2007;55:2957.
- [5] Hü bers HW. Richter H. Wienold M. High-resolution terahertz spectroscopy with quantum-cascade lasers. J Appl Phys. 2019;125(15):151401.
- Mittleman DM, Jacobsen RH, Neelamani R, Baraniuk RG, Nuss MC. [6] Gas sensing using terahertz time-domain spectroscopy. Appl Phys B. 1998;67:379.
- [7] Federici JF, Schulkin B, Huang F, Gary D, Barat R, Oliveira F, et al. THz imaging and sensing for security applications-explosives, weapons, and drugs. Semicond Sci Technol. 2005;20:S266.
- [8] Jepsen PU, Cooke DG, Koch M. Terahertz spectroscopy and imaging-Modern techniques and applications. Laser & Photonics Reviews. 2011;5(1):124-66.
- [9] Wubs J, Macherius U, Weltmann K, Lü X, Röben B, Biermann K, et al. Terahertz absorption spectroscopy for measuring atomic oxygen densities in plasmas. Plasma Sources Sci Technol. 2023;32(2):025006.
- Lü X, Röben B, Biermann K, Wubs J, Macherius U, Weltmann KD, et al. Terahertz quantum-cascade lasers for high-resolution absorption spectroscopy of atoms and ions in plasmas. Semicond Sci Technol. 2023;38:035003.
- Richter H, Wienold M, Schrottke L, Biermann K, Grahn HT, Hü [11] bers HW. 4.7-THz local oscillator for the GREAT heterodyne spectrometer on SOFIA. IEEE Trans Terahertz Sci Technol. 2015;5(4):539-45.
- [12] Gusdorf A, Anderl S, Lefloch B, Leurini S, Wiesemeyer H, Guesten R, et al. Nature of shocks revealed by SOFIA OI observations in the Cepheus E protostellar outflow. Astron Astrophys. 2017;602:A8.
- [13] Rezac L, Hartogh P, Güsten R, Wiesemeyer H, Hübers HW, Jarchow C, et al. First detection of the 63 μ m atomic oxygen line in the thermosphere of Mars with GREAT/SOFIA. Astron Astrophys. 2015;580:L10.
- [14] Richter H, Buchbender C, Gü sten R, Higgins R, Klein B, Stutzki J, et al. Direct measurements of atomic oxygen in the mesosphere and lower thermosphere using terahertz heterodyne spectroscopy. Commun Earth Environ. 2021;2(1):19.
- [15] Wiesemeyer H, Gü sten R, Aladro R, Klein B, Hü bers HW, Richter H, et al. First detection of the atomic O 18 isotope in the mesosphere and lower thermosphere of Earth. Phys Rev Res. 2023;5(1):013072.
- Krozer V, Loffler T, Dall J, Kusk A, Eichhorn F, Olsson RK, et al. Terahertz imaging systems with aperture synthesis techniques. IEEE Trans Microwave Theory Techniques. 2010;58(7):2027–39.
- Chan WL, Diebel J, Mittleman DM. Imaging with terahertz radiation. Rep Prog Phys. 2007;70:1325-79.
- Siegel PH. Terahertz technology in biology and medicine. IEEE Trans Microwave Theory Tech. 2004;52(10):2438-47.
- [19] Peng Y, Shi C, Wu X, Zhu Y, Zhuang S. Terahertz imaging and spectroscopy in cancer diagnostics: a technical review. BME Frontiers. 2020;2020:1-11.

- [20] Koenig S, Lopez-Diaz D, Antes J, Boes F, Henneberger R, Leuther A, et al. Wireless sub-THz communication system with high data rate. Nature Photonics. 2013;7(12):977.
- [21] Kleine-Ostmann T, Nagatsuma T. A review on terahertz communications research. J Infrared Millimeter Terahertz Waves. 2011;32(2):143-71.
- Chen Z, Ma X, Zhang B, Zhang Y, Niu Z, Kuang N, et al. A survey on [22] terahertz communications. China Commun. 2019:16(2):1-35.
- [23] Nagatsuma T, Ducournau G, Renaud CC. Advances in terahertz communications accelerated by photonics. Nature Photonics. 2016;10(6):371-9.
- [24] Sengupta K, Nagatsuma T, Mittleman DM. Terahertz integrated electronic and hybrid electronic-photonic systems. Nature Electronics. 2018:1(12):622-35.
- [25] Mehdi I. THz local oscillator technology. Proc. SPIE 5498, Millimeter and Submillimeter Detectors for Astronomy II. 2004.
- Ward J, Schlecht E, Chattopadhyay G, Maestrini A, Gill J, Maiwald F, [26] et al. Capability of THz sources based on Schottky diode frequency multiplier chains. IEEE MTT-S Int Microwave Symposium Digest. 2004;3:1587-90.
- [27] Siegel PH. Terahertz technology. IEEE Trans Microwave Theory Tech. 2002;50:910-28.
- [28] Woolard DL, Brown ER, Pepper M, Kemp M. Terahertz frequency sensing and imaging: a time of reckoning future applications? Proc IEEE. 2005;93:1722.
- [29] Yardimci NT, Jarrahi M. Nanostructure-enhanced photoconductive terahertz emission and detection. Small. 2018;14(44):1802437.
- Shi W, Ding YJ, Fernelius N, Vodopyanov K. Efficient, tunable, and [30] coherent 0.18-5.27-THz source based on GaSe crystal. Optics Letters. 2002;27(16):1454-6.
- Kawase K, Shikata J, Ito H. Terahertz wave parametric source. I Phys D Appl Phys. 2002;35(3):R1.
- [32] Fujita K, Jung S, Jiang Y, Kim JH, Nakanishi A, Ito A, et al. Recent progress in terahertz difference-frequency quantum cascade laser sources. Nanophotonics. 2018;7(11):1795-817.
- [33] Razeghi M, Lu Q, Bandyopadhyay N, Zhou W, Heydari D, Bai Y, et al. Quantum cascade lasers: from tool to product. Optics Express. 2015;23(7):8462-75.
- [34] Pflü gl C, Belkin MA, Wang QJ, Geiser M, Belyanin A, Fischer M, et al. Surface-emitting terahertz quantum cascade laser source based on intracavity difference-frequency generation. Appl Phys Lett. 2008;93(16):161110.
- Belkin MA, Capasso F, Belyanin A, Sivco DL, Cho AY, Oakley DC, et al. Terahertz quantum-cascade-laser source based on intracavity difference-frequency generation. Nature Photonics. 2007;1(5):288.
- [36] Lu Q, Razeghi M. Recent advances in room temperature, highpower terahertz quantum cascade laser sources based on difference-frequency generation. Photonics. 2016;3(3):42.
- Belkin MA, Capasso F. New frontiers in quantum cascade lasers: [37] high performance room temperature terahertz sources. Phys Scr. 2015:90(11):118002.
- [38] Jiang Y, Vijayraghavan K, Jung S, Jiang A, Kim JH, Demmerle F, et al. Spectroscopic study of terahertz generation in mid-infrared quantum cascade lasers. Scientific Reports. 2016;6:21169.
- Köhler R, Tredicucci A, Beltram F, Beere HE, Linfield EH, Davies AG, et al. Terahertz semiconductor-heterostructure laser. Nature. 2002;417(6885):156-9.

- [40] Walther C, Fischer M, Scalari G, Terazzi R, Hoyler N, Faist J. Quantum cascade lasers operating from 1.2 to 1.6 THz. Appl Phys Lett. 2007;91(13):131122.
- [41] Wienold M, Röben B, Lü X, Rozas G, Schrottke L, Biermann K, et al. Frequency dependence of the maximum operating temperature for quantum-cascade lasers up to 5.4 THz. Appl Phys Lett. 2015;107(20):202101.
- [42] Li L, Chen L, Freeman J, Salih M, Dean P, Davies A, et al. Multi-Watt high-power THz frequency quantum cascade lasers. Electron Lett. 2017;53(12):799–800.
- [43] Williams BS, Kumar S, Hu Q, Reno JL. High-power terahertz quantum-cascade lasers. Electron Lett. 2006;42:89.
- [44] Wang X, Shen C, Jiang T, Zhan Z, Deng Q, Li W, et al. High-power terahertz quantum cascade lasers with 0.23 W in continuous wave mode. AIP Adv. 2016;6(7):22194.
- [45] Vitiello MS, Scalari G, Williams B, De Natale P. Quantum cascade lasers: 20 years of challenges. Optics Express. 2015;23(4):5167–82.
- [46] Bosco L, Franckie M, Scalari G, Beck M, Wacker A, Faist J. Thermoelectrically cooled THz quantum cascade laser operating up to 210 K. Appl Phys Lett. 2019;115(1):010601.1–010601.5.
- [47] Khalatpour A, Paulsen AK, Deimert C, Wasilewski ZR, Hu Q. Highpower portable terahertz laser systems. Nature Photonics. 2020;15(1):1–5.
- [48] Khalatpour A, Tam MC, Addamane SJ, Reno J, Wasilewski Z, Hu Q. Enhanced operating temperature in terahertz quantum cascade lasers based on direct phonon depopulation. Appl Phys Lett. 2023;122(16):161101.
- [49] Fathololoumi S, Dupont E, Chan C, Wasilewski Z, Laframboise S, Ban D, et al. Terahertz quantum cascade lasers operating up to 200 K with optimized oscillator strength and improved injection tunneling. Optics Express. 2012;20(4):3866–76.
- [50] Kohen S, Williams BS, Hu Q. Electromagnetic modeling of terahertz quantum cascade laser waveguides and resonators. J Appl Phys. 2005:97:053106.
- [51] Belkin MA, Fan JA, Hormoz S, Capasso F, Linfield EH. Terahertz quantum cascade lasers with copper metal-metal waveguides operating up to 178 K. Optics Express. 2008;16(5):3242–8.
- [52] Williams BS, Kumar S, Hu Q, Reno JL. Distributed-feedback terahertz quantum-cascade lasers with laterally corrugated metal waveguides. Optics Letters. 2005;30(21):2909–11.
- [53] Kumar S, Williams BS, Qin Q, Lee AM, Hu Q, Reno JL. Surfaceemitting distributed feedback terahertz quantum-cascade lasers in metal-metal waveguides. Optics Express. 2007;15(1):113–28.
- [54] Amanti MI, Fischer M, Scalari G, Beck M, Faist J. Low-divergence single-mode terahertz quantum cascade laser. Nature Photonics. 2009;3:586–90.
- [55] Chassagneux Y, Colombelli R, Maineult W, Barbieri S, Beere HE, Ritchie DA, et al. Electrically pumped photonic-crystal terahertz lasers controlled by boundary conditions. Nature. 2009;457:174.
- [56] Mahler L, Tredicucci A, Beltram F, Walther C, Faist J, Witzigmann B, et al. Vertically emitting microdisk lasers. Nature Photonics. 2009;3:46.
- [57] Li H, Manceau J, Andronico A, Jagtap V, Sirtori C, Li L, et al. Coupled-cavity terahertz quantum cascade lasers for single mode operation. Appl Phys Lett. 2014;104(24):241102.
- [58] Hempel M, Röben B, Niehle M, Schrottke L, Trampert A, Grahn HT. Continuous tuning of two-section, single-mode terahertz quantum-cascade lasers by fiber-coupled, near-infrared illumination. AIP Adv. 2017;7(5):055201.

- [59] Yu N, Wang QJ, Kats MA, Fan JA, Khanna SP, Li L, et al. Designer spoof surface plasmon structures collimate terahertz laser beams. Nature Materials. 2010;9(9):730–5.
- [60] Zeng Y, Qiang B, Wang QJ. Photonic engineering technology for the development of terahertz quantum cascade lasers. Adv Opt Materials. 2020;8(3):1900573.
- [61] Curwen CA, Reno JL, Williams BS. Terahertz quantum cascade VECSEL with watt-level output power. Appl Phys Lett. 2018;113(1):011104.
- [62] Jin Y, Reno JL, Kumar S. Phase-locked terahertz plasmonic laser array with 2 W output power in a single spectral mode. Optica. 2020;7(6):708–15.
- [63] Khalatpour A, Reno JL, Hu Q. Phase-locked photonic wire lasers by π coupling. Nature Photonics. 2019;13(1):47–53.
- [64] Risacher C, Gü sten R, Stutzki J, Hü bers HW, Aladro R, Bell A, et al. The upGREAT dual frequency heterodyne arrays for SOFIA. J Astronom Instrument. 2018;07(04):1840014.
- [65] Vitiello MS, Tredicucci A. Tunable emission in THz quantum cascade lasers. IEEE Trans THz Sci Technol. 2011;1:76.
- [66] Qin Q, Williams BS, Kumar S, Hu Q, Reno JL. Tuning a terahertz wire laser. Nature Photonics. 2009;3:732–7.
- [67] Curwen CA, Reno JL, Williams BS. Broadband continuous singlemode tuning of a short-cavity quantum-cascade VECSEL. Nature Photonics. 2019;13(12):855–9.
- [68] Turčinková D, Amanti MI, Castellano F, Beck M, Faist J. Continuous tuning of terahertz distributed feedback quantum cascade laser by gas condensation and dielectric deposition. Appl Phys Lett. 2013;102(18):181113.
- [69] Wu C, Jin Y, Reno JL, Kumar S. Large static tuning of narrow-beam terahertz plasmonic lasers operating at 78 K. APL Photonics. 2017;2(2):026101.
- [70] Hempel M, Röben B, Schrottke L, Hü bers HW, Grahn HT. Fast continuous tuning of terahertz quantum-cascade lasers by rearfacet illumination. Appl Phys Lett. 2016;108(19):191106.
- [71] Ohtani K, Beck M, Faist J. Electrical laser frequency tuning by three terminal terahertz quantum cascade lasers. Appl Phys Lett. 2014:104(1):011107.
- [72] Dunbar LA, Houdré R, Scalari G, Sirigu L, Giovannini M, Faist J. Small optical volume terahertz emitting microdisk quantum cascade lasers. Appl Phys Lett. 2007;90:141114.
- [73] Zhang H, Scalari G, Faist J, Dunbar LA, Houdré R. Design and fabrication technology for high performance electrical pumped terahertz photonic crystal band edge lasers with complete photonic band gap. J Appl Phys.. 2010;108(9):093104.
- [74] Turčinková D, Amanti MI, Scalari G, Beck M, Faist J. Electrically tunable terahertz quantum cascade lasers based on a two-sections interdigitated distributed feedback cavity. Appl Phys Lett. 2015;106(13):131107.
- [75] Kundu I, Dean P, Valavanis A, Freeman JR, Rosamond MC, Li L, et al. Continuous frequency tuning with near constant output power in coupled Y-branched terahertz quantum cascade lasers with photonic lattice. ACS Photonics. 2018;5(7):2912–20.
- [76] Jenkins GS, Schmadel DC, Drew HD. Simultaneous measurement of circular dichroism and Faraday rotation at terahertz frequencies using heterodyne detection. Rev Scientif Instrum. 2010;81(8):140506.
- [77] Kan T, Isozaki A, Kanda N, Nemoto N, Konishi K, Takahashi H, et al. Enantiomeric switching of chiral metamaterial for terahertz polarization modulation employing vertically deformable MEMS spirals. Nature Commun. 2015;6:8422.

- [78] Peralta XG, Brener I, Padilla WJ, Young EW, Hoffman AJ, Cich MJ, et al. External modulators for terahertz quantum cascade lasers based on electrically-driven active metamaterials. Metamaterials. 2010;4(2–3):83–8.
- [79] Hsieh CF, Pan, RP, Tang, TT, Chen, HL, Pan, CL. Voltage-controlled liquid-crystal terahertz phase shifter and quarter-wave plate. Optics Lett. 2006;31(8):1112–4.
- [80] Yang CS, Tang TT, Chen PH, Pan RP, Pan CL. Voltage-controlled liquid-crystal terahertz phase shifter with indium-tin-oxide nanowhiskers as transparent electrodes. Optics Lett. 2014;39(8):2511–3.
- [81] RoSch M, Scalari G, Beck M, Faist J. Octave-spanning semiconductor laser. Nature Photonics. 2015;9(1):42–7.
- [82] Garrasi K, Mezzapesa FP, Salemi L, Li L, Consolino L, Bartalini S, et al. High dynamic range, heterogeneous, terahertz quantum cascade lasers featuring thermally tunable frequency comb operation over a broad current range. ACS Photonics. 2018;6(1):73–8.
- [83] Rösch M, Beck M, Sü ess MJ, Bachmann D, Unterrainer K, Faist J, et al. Heterogeneous terahertz quantum cascade lasers exceeding 1.9 THz spectral bandwidth and featuring dual comb operation. Nanophotonics. 2018;7(1):237–42.
- [84] Burghoff D, Kao TY, Han N, Chan CWI, Cai X, Yang Y, et al. Terahertz laser frequency combs. Nature Photonics. 2014;8(6):462–7.
- [85] Forrer A, Franckié M, Stark D, Olariu T, Beck M, Faist J, et al. Photon-driven broadband emission and frequency comb RF injection locking in THz quantum cascade lasers. ACS Photonics. 2020;7(3):784–91.
- [86] Di Gaspare A, Viti L, Beere HE, Ritchie DD, Vitiello MS. Homogeneous quantum cascade lasers operating as terahertz frequency combs over their entire operational regime. Nanophotonics. 2020;10(1):181–6.
- [87] Williams BS, Kumar S, Callebaut H, Hu Q, Reno JL. Terahertz quantum-cascade laser operating up to 137 K. Appl Phys Lett. 2003;83(25):5142–4.
- [88] Williams BS, Kumar S, Hu Q, Reno JL. Operation of terahertz quantum-cascade lasers at 164 K in pulsed mode and at 117 K in continuous-wave mode. Optics Express. 2005;13(9):3331–9.
- [89] Kumar S, Hu Q, Reno JL. 186 K operation of terahertz quantumcascade lasers based on a diagonal design. Appl Phys Lett. 2009;94(13):131105.
- [90] Williams BS, Kumar S, Callebaut H, Hu Q, Reno JL. Terahertz quantum-cascade laser at $\lambda \approx 100 \mu m$ using metal waveguide for mode confinement. Appl Phys Lett. 2003;83(11):2124–6.
- [91] Hagelschuer T, Richter H, Wienold M, Lü X, Röben B, Schrottke L, et al. A compact 4.75-THz source based on a quantum-cascade laser with a back-facet mirror. IEEE Trans Terahertz Sci Technol. 2019;9(6):606–12.
- [92] Bosco L, Bonzon C, Ohtani K, Justen M, Beck M, Faist J. A patcharray antenna single-mode low electrical dissipation continuous wave terahertz quantum cascade laser. Appl Phys Lett. 2016;109(20):201103.
- [93] Justen M, Bonzon C, Ohtani K, Beck M, Graf U, Faist J. 2D patch antenna array on a double metal quantum cascade laser with >90% coupling to a Gaussian beam and selectable facet transparency at 1.9 THz. Optics Lett. 2016;41(19):4590–2.
- [94] Walker CK, Kulesa CA, Young A, Verts WT, Gao J, Hu Q, et al. Gal/ Xgal U/LDB spectroscopic/stratospheric THz observatory: GUSTO.

- Proc. SPIE 12190, Millimeter, Submillimeter, and Far-Infrared Detectors and Instrumentation for Astronomy XI, 121900E. 2022.
- [95] Khalatpour A, Paulsen AK, Addamane SJ, Deimert C, Reno JL, Wasilewski ZR, et al. A Tunable Unidirectional Source for GUSTOas Local Oscillator at 4.74 THz. IEEE Trans Terahertz Sci Technol. 2021;12(2):144–50.
- [96] Schrottke L, Lü X, Rozas G, Biermann K, Grahn HT. Terahertz GaAs/AlAs quantum-cascade lasers. Appl Phys Lett. 2016;108(10):102102.
- [97] Schrottke L, Röpcke J, Grahn HT, Lü X, Röben B, Biermann K, et al. High-performance GaAs/AlAs terahertz quantum-cascade lasers for spectroscopic applications. IEEE Trans Terahertz Sci Technol. 2019:10(2):133-40.
- [98] Schrottke L, Wienold M, Sharma R, Lü X, Biermann K, Hey R, et al. Quantum-cascade lasers as local oscillators for heterodyne spectrometers in the spectral range around 4.745 THz. Semiconductor Sci Technol. 2013;28(3):035011.
- [99] Ren Y, Wallis R, Jessop DS, Degl'Innocenti R, Klimont A, Beere HE, et al. Fast terahertz imaging using a quantum cascade amplifier. Appl Phys Lett. 2015;107(1):011107.
- [100] Rakic A, Taimre T, Bertling K, Lim Y, Dean P, Valavanis A, et al. Sensing and imaging using laser feedback interferometry with quantum cascade lasers. Appl Phys Rev. 2019;6(2):021320.
- [101] Dean P, Valavanis A, Keeley J, Bertling K, Lim YL, Alhathlool R, et al. Terahertz imaging using quantum cascade lasers-a review of systems and applications. J Phys D Appl Phys. 2014;47(37):374008.
- [102] Yang Y, Burghoff D, Hayton DJ, Gao JR, Reno JL, Hu Q. Terahertz multiheterodyne spectroscopy using laser frequency combs. Optica. 2016;3(5):499–502.
- [103] Asaf A, Qing H. Carrier leakage into the continuum in diagonal GaAs/Al0.15GaAs terahertz quantum cascade lasers. Appl Phys Lett. 2015;107(24):3866–2.
- [104] Faist J. Wallplug efficiency of quantum cascade lasers: Critical parameters and fundamental limits. Appl Phys Lett. 2007;90(25):253512.
- [105] Faist J, Scalari G. Unified description of resonant tunnelling diodes and terahertz quantum cascade lasers. Electron Lett. 2010;46(26):S46–9.
- [106] Li L, Chen L, Zhu J, Freeman J, Dean P, Valavanis A, et al. Terahertz quantum cascade lasers with > 1 W output powers. Electron Lett. 2014;50(4):309–11.
- [107] Lin TT, Wang L, Wang K, Grange T, Birner S, Hirayama H. Over one Watt output power terahertz quantum cascade lasers by using high doping concentration and variable barrier-well height. Physica Status Solidi (RRL)-Rapid Res Lett. 2022;16(7):2200033.
- [108] Richter H, Semenov A, Pavlov S, Mahler L, Tredicucci A, Beere HE, et al. Terahertz heterodyne receiver with quantum cascade laser and hot electron bolometer mixer in a pulse tube cooler. Appl Phys Lett. 2008;93(14):141108.
- [109] Richter H, Rothbart N, Hü bers HW. Characterizing the beam properties of terahertz quantum-cascade lasers. J Infrared Millimeter Terahertz Waves. 2014;35:686–98.
- [110] Lee AWM, Qin Q, Kumar S, Williams BS, Hu Q, Reno JL. High-power and high-temperature THz quantum-cascade lasers based on lens-coupled metal-metal waveguides. Optics Lett. 2007;32(19):2840–2.
- [111] Wan W, Li H, Cao J. Homogeneous spectral broadening of pulsed terahertz quantum cascade lasers by radio frequency modulation. Optics Express. 2018;26(2):980–9.

- [112] Xu G, Colombelli R, Khanna SP, Belarouci A, Letartre X, Li L, et al. Efficient power extraction in surface-emitting semiconductor lasers using graded photonic heterostructures. Nature Comm. 2012;3:952.
- [113] Jin Y, Gao L, Chen J, Wu C, Reno JL, Kumar S. High power surface emitting terahertz laser with hybrid second-and fourth-order Bragg gratings. Nature Commun. 2018;9(1):1–7.
- [114] Chen J, Gao L, Jin Y, Reno JL, Kumar S. High-intensity and low-divergence THz laser with 1D autofocusing symmetric Airy beams. Optics Express. 2019;27(16):22877–89.
- [115] Xu L, Curwen C, Chen D, Reno J, Itoh T, Williams B. Terahertz metasurface quantum-cascade VECSELs: theory and performance. IEEE J Selected Topics Quantum Electron. 2017;23(6):1–12.
- [116] Burghoff D, Chan CWI, Hu Q, Reno JL. Gain measurements of scattering-assisted terahertz quantum cascade lasers. Appl Phys Lett. 2012;100:261111.
- [117] Bachmann D, Roesch M, Deutsch C, Krall M, Scalari G, Beck M, et al. Spectral gain profile of a multi-stack terahertz quantum cascade laser. Appl Phys Lett. 2014;105(18):156.
- [118] Qi Q, Reno JL, Hu Q. MEMS-based tunable terahertz wire-laser over 330GHz. Optics Lett. 2011;36(5):692–4.
- [119] Mahler L, Köhler R, Tredicucci A, Beltram F, Beere HE, Linfield EH, et al. Single-mode operation of terahertz quantum cascade lasers with distributed feedback resonators. Appl Phys Lett. 2004;84(26):5446–8.
- [120] Wienold M, Tahraoui A, Schrottke L, Sharma R, Lü X, Biermann K, et al. Lateral distributed-feedback gratings for single-mode, highpower terahertz quantum-cascade lasers. Optics Express. 2012;20(10):11207–17.
- [121] Kao TY, Hu Q, Reno JL. Perfectly phase-matched third-order distributed feedback terahertz quantum-cascade lasers. Optics Letters. 2012;37(11):2070–2.
- [122] Zhang H, Dunbar LA, Scalari G, Houdré R, Faist J. Terahertz photonic crystal quantum cascade lasers. Optics Express. 2007;15(25):16818–27.
- [123] Diao Z, Bonzon C, Scalari G, Beck M, Faist J, Houdré R. Continuous-ÂŘwave vertically emitting photonic crystal terahertz laser. Laser Photonics Reviews. 2013;7:L45–50.
- [124] Halioua Y, Xu G, Moumdji S, Li LH, Davies AG, Linfield EH, et al. THz quantum cascade lasers operating on the radiative modes of a 2D photonic crystal. Optics Lett. 2014;39(13):3962–5.
- [125] Röben B, Lü X, Biermann K, Schrottke L, Grahn H. Terahertz quantum-cascade lasers for high-resolution spectroscopy of sharp absorption lines. J Appl Phys. 2019;125(15):151613.
- [126] Alam T, Wienold M, Lü X, Biermann K, Schrottke L, Grahn HT, et al. Wideband, high-resolution terahertz spectroscopy by light-induced frequency tuning of quantum-cascade lasers. Optics Express. 2019;27(4):5420–32.
- [127] Gao L, Zhao L, Reno JL, Kumar S. Electrical tuning of a terahertz quantum cascade laser based on detuned intersubband absorption. Appl Phys Lett. 2019;115(14):141102.
- [128] Maineult W, Ding L, Gellie P, Filloux PG, Sirtori C, Barbieri S, et al. Microwave modulation of terahertz quantum cascade lasers: a transmission-line approach. Appl Phys Lett. 2010;96(2):021108.
- [129] Kundu I, Freeman JR, Dean P, Li LH, Davies AG. Wideband electrically controlled Vernier frequency tunable terahertz quantum cascade laser. ACS Photonics. 2020;7(3):765–73.

- [130] Zhu H, Zhu H, Wang K, Yu C, He L. Terahertz master-oscillator power-amplifier quantum Cascade laser with controllable polarization. Appl Phys Lett. 2020;117(2):021103.
- [131] Pérez-Urquizo J, Todorov Y, Li L, Davies AG, Linfield EH, Sirtori C, et al. Monolithic patch-antenna THz lasers with extremely low beam divergence and polarization control. ACS Photonics. 2021;8(2):412–7.
- [132] Liang G, Zeng Y, Hu X, Yu H, Liang H, Zhang Y, et al. Monolithic semiconductor lasers with dynamically tunable linear-to-circular polarization. ACS Photonics. 2017;4(3):517–24.
- [133] Xu L, Chen D, Curwen C, Memarian M, Reno J, Itoh T, et al. Metasurface quantum-cascade lasers with electrically switchable polarization. Optica. 2017;4(4):468–75.
- [134] Rauter P, Lin J, Genevet P, Khanna SP, Lachab M, Giles Davies A, et al. Electrically pumped semiconductor laser with monolithic control of circular polarization. Proceedings of the National Academy of Sciences of the United States of America. 2014;111(52):E5623–32.
- [135] Li L, Garrasi K, Kundu I, Han Y, Salih M, Vitiello M, et al. Broadband heterogeneous terahertz frequency quantum cascade laser. Electron Lett. 2018;54(21):1229–31.
- [136] Faist J, Villares G, Scalari G, Rösch M, Bonzon C, Hugi A, et al. Quantum cascade laser frequency combs. Nanophotonics. 2016;5(2):272–91.
- [137] Khurgin J, Dikmelik Y, Hugi A, Faist J. Coherent frequency combs produced by self frequency modulation in quantum cascade lasers. Appl Phys Lett. 2014;104(8):081118.
- [138] Vitiello MS, Consolino L, Inguscio M, De Natale P. Toward new frontiers for terahertz quantum cascade laser frequency combs. Nanophotonics. 2020;10(1):187–94.
- [139] Burghoff D, Yang Y, Hayton DJ, Gao JR, Reno JL, Hu Q. Evaluating the coherence and time-domain profile of quantum cascade laser frequency combs. Optics Express. 2015;23(2):1190–202.
- [140] Yang Y, Burghoff D, Reno J, Hu Q. Achieving comb formation over the entire lasing range of quantum cascade lasers. Optics Lett. 2017;42(19):3888–91.
- [141] Consolino L, Nafa M, Regis MD, Cappelli F, Garrasi K, Mezzapesa FP, et al. Quantum cascade laser based hybrid dual comb spectrometer. Commun Phys. 2020;3(1):69.
- [142] Sterczewski LA, Westberg J, Yang Y, Burghoff D, Reno J, Hu Q, et al. Terahertz spectroscopy of gas mixtures with dual quantum cascade laser frequency combs. ACS Photonics. 2020;7(5):1082–7.
- [143] Kazakov D, Piccardo M, Wang Y, Chevalier P, Mansuripur TS, Xie F, et al. Self-starting harmonic frequency comb generation in a quantum cascade laser. Nature Photonics. 2017;11(12):789–92.
- [144] Gaspare AD, Pogna EAA, Salemi L, Balci O, Cadore AR, Shinde SM, et al. Tunable, Grating-Gated, Graphene-On-Polyimide Terahertz Modulators. Adv Funct Materials. 2021;31(10):2008039.
- [145] Mezzapesa FP, Garrasi K, Schmidt J, Salemi L, Pistore V, Li L, et al. Terahertz frequency combs exploiting an on-chip, solution-processed, graphene-quantum cascade laser coupled-cavity. ACS photonics. 2020;7(12):3489–98.
- [146] Mezzapesa FP, Viti L, Li L, Pistore V, Dhillon S, Davies AG, et al. Chip-Scale Terahertz Frequency Combs through Integrated Intersubband Polariton Bleaching. Laser Photonics Reviews. 2021;15(6):2000575.
- [147] Vitiello MS, De Natale P. Terahertz quantum cascade lasers as enabling quantum technology. Adv Quantum Technol. 2022;5(1):2100082.

- [148] Sun G, Soref RA, Khurgin JB. Active region design of a terahertz GaN/Al0. 15Ga0. 85N quantum cascade laser. Superlattices Microstruct. 2005;37(2):107-13.
- [149] Wang L, Lin TT, Chen MX, Wang K, Hirayama H. Engineering of electron-longitudinal optical phonon coupling strength in mplane GaN terahertz quantum cascade lasers. Appl Phys Express. 2021;14(11):112003.
- [150] Terashima W, Hirayama H. GaN-based terahertz quantum cascade lasers. Proc. SPIE 9483, Terahertz Physics, Devices, and Systems IX: Advanced Applications in Industry and Defense. 2015.
- [151] Paul DJ. The progress towards terahertz quantum cascade lasers on silicon substrates. Laser Photonics Rev. 2010;4(5):610-32.
- [152] Grange T, Stark D, Scalari G, Faist J, Virgilio M. Room temperature operation of n -type Ge/SiGe terahertz quantum cascade lasers predicted by non-equilibrium Green's functions. Appl Phys Lett. 2019;114(11):111102.
- Liang G, Hu X, Yu X, Shen Y, Li L, Davies AG, et al. Integrated [153] terahertz graphene modulator with 100% modulation depth. ACS Photonics. 2015;2(11):1559-66.